Draft version May 16, 2011
Preprint typeset using LaTeX style emulateapj v. 11/10/09

AEGIS: THE MORPHOLOGIES OF GREEN GALAXIES AT $0.4 < Z < 1.2$

Alexander J. Mendez [1], Alison L. Coil[1,2], Jennifer Lotz[3], Samir Salim[3], John Moustakas[1], Luc Simard[4]

Draft version May 16, 2011

ABSTRACT

We present quantitative morphologies of ∼300 galaxies in the optically-defined green valley at $0.4 < z < 1.2$, in order to constrain the mechanism(s) responsible for quenching star formation in the bulk of this population. The sample is selected from galaxies in the All-Wavelength Extended Groth Strip International Survey (AEGIS). While the green valley is defined using optical U-B colors, we find that using a green valley sample defined using NUV-R colors does not change the results. Using *HST*/ACS imaging, we study several quantitative morphological parameters including CAS, B/T from GIM2D, and Gini/M_{20}. We find that the green galaxy population is intermediate between the red and blue galaxy populations in terms of concentration, asymmetry, and morphological type and merger fraction estimated using Gini/M_{20}. We find that most green galaxies are *not* classified as mergers; in fact, the merger fraction in the green valley is *lower* than in the blue cloud. We show that at a given stellar mass, green galaxies have higher concentration values than blue galaxies and lower concentration values than red galaxies. Additionally, we find that 12% of green galaxies have $B/T = 0$ and 21% with $B/T \leq 0.05$. Our results show that green galaxies are generally massive ($M_* \sim 10^{10.5}$ $M_\odot$) disk galaxies with high concentrations. We conclude that major mergers are likely not the sole mechanism responsible for quenching star formation in this population and that either other external processes or internal secular processes play an important role both in driving gas towards the center of these galaxies and in quenching star formation.

1. INTRODUCTION

The wealth of data generated by local large redshift surveys such as the *Sloan Digital Sky Survey* (SDSS, York et al. 2000) and the *Two-Degree Field Galaxy Redshift Survey* (2dFGRS, Colless et al. 2001) have greatly advanced our understanding of galaxy properties at $z \sim 0.1$. These surveys have clearly established that the local galaxy population exhibits a bimodal distribution in terms of optical color (e.g., Strateva et al. 2001; Blanton et al. 2003), UV-optical color (Salim et al. 2007), the 4000Å break $D_n - 4000$ (Kauffmann et al. 2003), and spectral type (Madgwick et al. 2002). In optical color-magnitude diagrams (CMDs) galaxies predominantly lie along either the "red sequence", which is dominated by quiescent, non-star-forming, early-type, bulge-dominated galaxies (e.g., Zhu, Blanton, & Moustakas 2010; Blanton & Moustakas 2009), or in the "blue cloud," characterized by star-forming, late-type, disk-dominated galaxies.

Deeper redshift surveys that probe galaxies at an earlier stage of evolution have shown that this bimodality exists at least to $z \sim 2$ (e.g., Willmer et al. 2006; Faber et al. 2007; Kriek et al. 2008; Williams et al. 2009). The location of the bimodality minimum is bluer at $z \sim 1$ by approximately 0.1 mag, as both blue and red galaxies were bluer in the past (Blanton 2006). Results from the COMBO-17 (Bell et al. 2004) and NOAO Deep Wide-Field Survey (Brown et al. 2007) photometric redshift surveys and the DEEP2 spectroscopic redshift survey (Faber et al. 2007) show that the red sequence has grown in mass by a factor of 2-4 since $z \sim 1$, while the number density of galaxies in the blue cloud has remained roughly constant (Bell et al. 2004; Brown et al. 2007; Faber et al. 2007). The large influx of red sequence galaxies brighter than L_* at $z \leq 0.7$ is dominated by spheroidal systems (Blanton et al. 2003; Bell et al. 2006; Weiner et al. 2005; Scarlata et al. 2007), but red disk-dominated galaxies are more common at fainter magnitudes (Brown et al. 2007).

Recent observational studies investigating galaxies in the minimum of the optical color bimodality, so-called "green valley" galaxies, have begun to probe the nature of this population. Baldry et al. (2004) model the u-r color distribution of SDSS galaxies and find that it can be fit as the sum of separate Gaussian distributions for the red and blue populations, implying that green valley galaxies are not necessarily a distinct population. However, Wyder et al. (2007) use UV-optical colors to more clearly separate the star-forming and quiescent populations and show that there is an excess of galaxies in the green valley galaxy population at $z \sim 0.1$; thus green galaxies may not be a simple mix of blue and red galaxies. Additionally, Salim et al. (2009) show in a comparison of the specific star formation rate (SSFR) versus rest-frame UV-optical color for low redshift galaxies that there is a smooth transition from high to low SSFR as color increases; galaxies at intermediate colors do not have a SSFR distribution that encompasses the values seen for both red and blue galaxies and thus appear to be a transition population.

The observed bimodality of galaxy colors reflects the fact that galaxies are either actively forming stars and are optically blue, are not forming stars and are optically red, or are dusty. After a galaxy stops forming stars, it should

[1] Department of Physics, University of California San Diego, 9500 Gilman Dr., La Jolla, CA 92093
[2] Alfred P. Sloan Foundation Fellow
[3] National Optical Astronomical Observatory, 950 North Cherry Ave., Tucson, AZ 85719
[4] National Research Council of Canada, Herzberg Institute of Astrophysics, 5071 West Saanich Road, Victoria, British Columbia, V9E 2E7, Canada

move from the blue cloud to the red sequence; star formation quenching could therefore explain the observed evolutionary trends. From the observed number densities and clustering properties of galaxies as a function of color, the implied timescale for movement to the red sequence after the quenching of star formation must be short, on the order of ~ 1 Gyr, otherwise there would be no observed bimodality (Faber et al. 2007; Martin et al. 2007; Tinker, Wechsler, & Zheng 2010). The short time scale is also a natural consequence of stellar population models; without star formation blue galaxies turn red in ~ 1 Gyr (Bruzual & Charlot 2003).

It is not yet known what physical mechanism or mechanisms cause these galaxies to stop forming stars. A variety of star formation quenching mechanisms have been proposed. It has long been suggested that major mergers are the dominant mechanism responsible for converting blue, star-forming, spiral galaxies into red, quiescent, elliptical galaxies. Simulations show that major mergers randomize the orbits of stars within a galaxy and can change the overall galaxy morphology from a disk into a bulge (e.g. Toomre & Toomre 1972; Toomre 1977; Barnes & Hernquist 1992; Hernquist 1992, 1993; Naab & Burkert 2003; Cox et al. 2006b). During the merger, gas is funneled to the center of the remnant, resulting in a burst of star formation that consumes, expels and/or heats some fraction of the available gas through shocks or feedback from supernovae (e.g. Barnes & Hernquist 1996; Springel, Di Matteo, & Hernquist 2005b; Robertson et al. 2006; Cox et al. 2006a; Steinmetz & Navarro 2002).

Merger-induced starbursts alone are likely insufficient to fully quench star formation or to consume *all* of the available gas, particularly for gas rich mergers at high redshift; additional quenching or gas removal is needed (Dekel & Birnboim 2006; Birnboim, Dekel, & Neistein 2007). Cox et al. (2008) show that in smoothed particle hydrodynamic simulations the starburst efficiency in merger-induced starbursts in recent simulations is lower than what was found previously. Their results suggest that these starbursts will not fully consume or eject all of the gas in the system. Additionally, Lotz et al. (2008a) use similar simulations to show that major merger remnants have enhanced SFR for $\sim$1 Gyr *after* the coalescence of the nuclei, indicating that additional gas removal mechanisms are required. Residual star formation in the remnant can prevent the galaxy from having red colors characteristic of elliptical galaxies (Springel, Di Matteo, & Hernquist 2005a). In order for the green valley to exist, star formation must be quenched on relatively short time scales, of order $\sim$1 Gyr. If instead the residual star formation declines slowly over a Hubble time (Mihos & Hernquist 1994), the remnant would gradually transition to the red sequence, removing the green valley distinction between the red and blue galaxy populations.

Further, simulations show that cold gas accretion from the intergalactic medium can also feed star formation in galaxies, particularly at high redshift (Dekel & Birnboim 2006; Birnboim, Dekel, & Neistein 2007; Kereš et al. 2005, 2009; Brooks et al. 2009). In these simulations, dense filamentary gas collapses to forms cold clouds which are stable against shocks and can penetrate to the centers of dark matter halos and accrete onto galaxies. This cold gas inflow further necessitates additional quenching mechanisms, as red and dead galaxies must remain quenched for the majority of cosmic time. Shock heating of the gas as it falls into a more massive dark matter halo limits the cold gas accretion from the intergalactic medium. For halos with masses above $\sim 10^{12}$ $M_{\odot}$, the infalling gas is heated to such a temperature that the cooling time is longer than the Hubble time, so that it cannot radiatively cool, thereby forming a halo of hot gas (Birnboim & Dekel 2003; Kereš et al. 2005; Dekel & Birnboim 2006). Johansson, Naab, & Ostriker (2009) show that gravitational heating may also be an important mechanism in massive halos, through the release of potential energy from infalling stellar clumps.

In addition to shock heating of infalling gas, Croton et al. (2006) has incorporated "radio-mode" Active galactic nucleus(AGN) feedback into simulations, in which an AGN heats gas in massive structures, such as galaxy groups and clusters to limit intergalactic gas from being able fall into the galaxy. This form of AGN feedback is observationally supported by X-ray imaging of evacuated cavities around massive galaxies in the centers of clusters (McNamara et al. 2000, 2001; McNamara & Nulsen 2007). Quasar mode AGN feedback, invoked in many current galaxy evolution models (Hopkins et al. 2006; Davé et al. 2001), could potentially limit the amount of cold gas available for star formation, but there is little direct observational evidence for this picture.

Interestingly, the rate of AGN detection is high in green valley galaxies, whether AGN are selected by deep X-ray surveys (Nandra et al. 2007; Coil et al. 2009; Hickox et al. 2008; Schawinski et al. 2009; Cardamone et al. 2010) or by optical line-ratio diagnostics (Salim et al. 2007). Nandra et al. (2007) find that many X-ray AGN host galaxies are green defined using (U-B) colors, while Pierce et al. (2010) find the same trend using (NUV-R) colors. Coil et al. (2008) show that in coadded spectra of DEEP2 galaxies, the average spectrum of green galaxies at $z \sim 1$ is not a simple mix of the average spectra of blue and red galaxies but instead shows line ratios indicative of enhanced AGN activity. Additionally, Bundy et al. (2008) find that the star formation quenching rate from $z \sim 1$ to today is consistent with the AGN "trigger" rate. It remains unclear, however, whether the presence of an AGN in a green valley galaxy is directly related to the star formation quenching process.

On the observational side, much recent work shows that secular effects may also play a crucial role in establishing the color bimodality. The majority of nearby disk galaxies ($\sim$ 75%) are found to have a stellar bar (Eskridge et al. 2000; Menéndez-Delmestre et al. 2007), and the bar fraction remains high to $z \sim 1$ (Sheth et al. 2003; Elmegreen, Elmegreen, & Hirst 2004; Jogee et al. 2004). The large non-axially-symmetric potential of bar galaxies can induce a large-scale inflow of stars and gas (Sellwood & Wilkinson 1993; Sheth et al. 2005), and studies of gas kinematics in the bar indicate that molecular gas flows inward along the bar dust lanes (Downes et al. 1996; Regan, Sheth, & Vogel 1999; Sheth et al. 2000; Sheth & Tormen 2002). Additionally, López-Sanjuan et al. (2010b) find that minor

mergers can not fully account for the mass growth of galaxies, suggesting that secular processes are needed to generate a bulge-dominated population. These bulge-dominated galaxies may be populating early-type spirals such as those observed by Bundy et al. (2010). Interestingly, Masters et al. (2010) and Cameron et al. (2010) find that early-type spirals have higher bar fractions than late-types spirals. At $z \sim 1$ Oesch et al. (2010) and López-Sanjuan et al. (2010a) find that major mergers are not common enough to explain the late- to early-type transition and suggest that either minor mergers or secular processes are needed.

Other potential quenching mechanisms need to have enough energy to halt star formation and continue to keep star formation quenched over a Hubble time. Many of the proposed mechanisms either heat the gas such that it cannot collapse to form stars (e.g. AGN feedback, Bower et al. 2006; Croton et al. 2006; Hopkins et al. 2006; Kang, Jing, & Silk 2006; Springel, Di Matteo, & Hernquist 2005a), remove cold gas from the galaxy as it falls into a halo (e.g. ram-pressure stripping Gunn & Gott 1972; Kimm et al. 2009; Quilis, Moore, & Bower 2000; Hester 2006; Farouki & Shapiro 1980; Moore et al. 1996; Abadi, Moore, & Bower 1999), or remove hot, diffuse, gas from a satellite galaxy (e.g. "strangulation" Larson, Tinsley, & Caldwell 1980; Balogh, Navarro, & Morris 2000). Tidal stripping of gas along the orbit of a satellite galaxy both removes gas and causes the galaxy to become more concentrated (van den Bosch et al. 2008), unlike ram-pressure stripping and strangulation, which mainly influence the gas in the galaxy as opposed to the stars. Additionally, gravitational interactions can greatly alter the morphology and gas content of a galaxy from the cumulative effect of many high-speed impulsive encounters, known as "harassment" (Farouki & Shapiro 1981; Moore et al. 1996).

The variety of proposed star formation quenching mechanisms mentioned above should have different morphological consequences. Therefore, in principle, one should be able to study the morphologies of green valley galaxies to constrain the dominant quenching mechanism. For example, parametric measures such as galaxy asymmetry can identify disturbed morphologies caused by major mergers (Conselice, Bershady, & Jangren 2000). In addition, the Gini coefficient (G) and second-order moment of light (M_{20}) parameters can be used to identify both major and minor mergers (Lotz et al. 2010). Gas stripping should lead to galaxies with truncated disks (Moore et al. 1996), while enhanced star formation due to harassment or other environmental interactions should lead to localized luminous areas, increasing the clumpiness (and decreasing the smoothness) of galaxies (Moore, Lake, & Katz 1998).

Previous studies of morphology and color have found that while most red galaxies have early-type, bulge-dominated morphologies, morphologically intermediate-type galaxies (type Sa-Sbc) are scattered throughout the CMD, including the red sequence (e.g., Ball et al. 2006; Driver et al. 2006; Bell et al. 2003; Blanton & Moustakas 2009; Pannella et al. 2009). It is not yet clear if the majority of galaxies on the red sequence were already spheroidal when they first joined the red sequence or if they were still disk-dominated and later became spheroidal through mergers with other red galaxies, or if a combination of both processes occurs (Faber et al. 2007). Galaxies could potentially also move from the red sequence to the blue cloud, for example as the result of a merger between a blue and red galaxy. However, the bulk of the movement must be from the blue cloud to the red sequence to explain the observed mass and number density evolution on the red sequence.

In this paper we investigate the morphologies of green valley galaxies at $z \sim 1$ to a) compare their morphological distributions to those of blue and red galaxies at the same redshift, to constrain the dominant star formation quenching mechanism(s) at work, and b) test whether the morphological distribution of green galaxies is consistent with being a simple mix of red and blue galaxies, or whether green galaxies have a distinct morphological makeup. We use a sample of galaxies at $0.4 < z < 1.2$ from the All-Wavelength Extended Groth Strip International Survey (AEGIS) (Davis et al. 2007), combining *HST*/ACS imaging with DEEP2 spectroscopic and CFHTLS photometric redshifts to measure various quantitative morphological parameters.

The outline of the paper is as follows: In §2 we present the AEGIS datasets used here. In §3 we define the red, green and blue samples used here. In §4 we discuss the different morphological parameters measured. In §5 we present results on the morphologies of green galaxies compared to the red and blue galaxies at the same redshift. In §6 we perform statistical tests with control samples of blue and red galaxies to determine whether the green galaxy population has a distinct morphological distribution. Finally, we discuss and summarize the results in §7. Absolute magnitudes given in this paper are in the AB system and are $M_B - 5\log(h)$ with $h = 0.7$, which for the remainder of the paper we denote as M_B. We assume the standard flat ΛCDM model with $\Omega_m = 0.3$ and $\Omega_\Lambda = 0.7$.

2. DATA

To quantify the morphological distribution of green valley galaxies, we require a large, complete parent sample of galaxies with accurate redshifts, rest-frame colors and magnitudes, and high-resolution imaging. As galaxies in the green valley have a lower space density than either blue or red galaxies, we require a large parent sample to measure the bivariate distribution of morphological parameters with sufficient objects per bin. We use data from the AEGIS survey (Davis et al. 2007), which covers the Extended Groth Strip (EGS) and contains DEEP2 spectroscopic and CFHTLS photometric redshifts. We use *HST*/ACS imaging and CFHTLS photometry to define a complete galaxy sample large enough to allow us to quantify the joint morphological properties of green galaxies. We further use *GALEX* photometry in the field to test the effects of excluding green galaxies that are likely dusty, star-forming blue galaxies, as opposed to true transitionary galaxies. Table 1 contains a summary of the datasets and sample sizes.

2.1. HST/*ACS Imaging*

High-resolution images from the Hubble Space Telescope (*HST*) Advanced Camera for Surveys (ACS) were

TABLE 1
Summary of Data Sets

Survey	Wavelengths/Bands	Sample Size [a]	Survey Limit
HST/ACS Imaging	*V*	2437	28.75(V_{AB})
"	*I*	2437	28.10(I_{AB})
DEEP2 Spectroscopic Redshifts	6400-9100Å	1220	24.1 (R_{AB})
CFHTLS Photometric Redshifts	*ugriz*	2324	25.(i_{AB})
GALEX Deep Imaging Survey	*NUV*	1021	26.5(AB)
"	*FUV*	345	25(AB)
CFHT Legacy Survey Photometry	*ugriz*	2437	∼27(AB)

[a] Number of galaxies with redshift with $0.4 < z < 1.2$, average signal-to-noise per pixel greater than 4, Petrosian radius $r_p > 0.3''$, and $M_B > -18$.

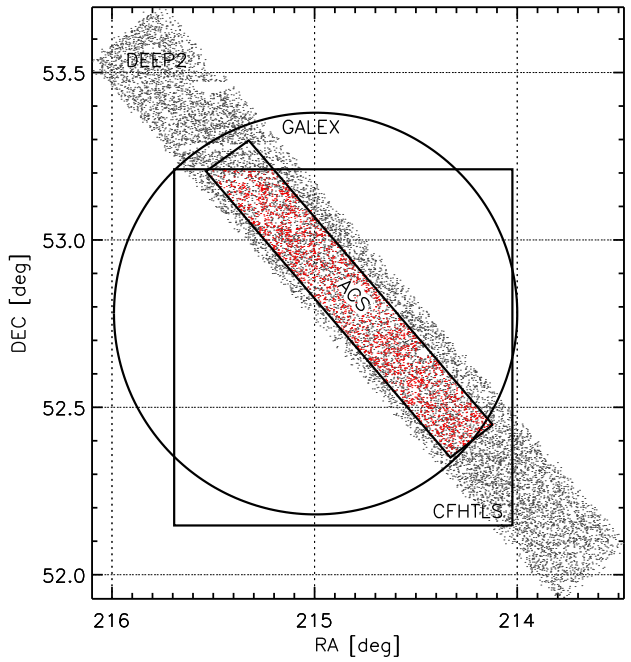

Fig. 1.— Areal map of the various relevant datasets in the EGS. Individual DEEP2 galaxies are shown in black points to a limit of to $R_{\rm AB} < 24.1$ and our sample is shown in red. Here we use galaxies that lie within the ACS region of the EGS and have secure DEEP2 spectroscopic redshifts (grey points) or good CFHTLS photometric redshifts (square region), with additional cuts (see Table 1 for sample sizes and depths). A single 1 deg deep *GALEX* pointing also overlaps a majority of the region.

obtained from the AEGIS survey as part of the GO Program, 10134 PI: M. Davis (Davis et al. 2007). The EGS was imaged in both the *V* (F606 W, 2260 sec) and *I* (F814W, 2100 sec) bands in a ∼10.′1 by 67.′ strip along the field. For details about the ACS imaging and reduction see Davis et al. (2007) and Lotz et al. (2008b). The 5σ limiting magnitudes for a point source are $V_{\rm AB} = 28.75$ and $I_{\rm AB} = 28.10$.

2.2. *CFHTLS ugriz Photometry*

We use CFHTLS T0004 release *ugriz* photometry (Ilbert et al. 2006) to calculate rest-frame colors and magnitudes for each galaxy. The CFHTLS Deep Field 3 is a $1^\circ \times 1^\circ$ field that covers the majority of the ACS region (see Figure 1). We use CFHTLS photometry, flux limited to $i_{\rm AB} < 25$, for objects in the ACS region, to calculate rest frame magnitudes. There are 16,450 objects in the ACS footprint with CFHTLS *ugriz* photometry.

2.3. GALEX *NUV/FUV Photometry*

We use near-UV (NUV) and far-UV (FUV) data obtained from the single 1.°2 diameter pointing of the central region of the EGS, taken with the *Galaxy Evolution Explorer* (*GALEX*; Martin et al. 2005; Morrissey et al. 2007). The 237 ks of NUV imaging and 120 ks of FUV imaging data are part of the third data release (GR3) (Zamojski et al. 2007). We use deblended *GALEX* photometry from Salim et al. (2009), which use an expectation maximization (EM) method to measure fluxes using a Bayesian deblending technique (Guillaume et al. 2006) and optical *u*-band priors (see Salim et al. 2009, for details). This method overcomes issues of blending and source confusion due to the $4''$-$5''$ spatial resolution (FWHM) of *GALEX* (Morrissey et al. 2007). NUV detections are measured to a flux limit of $NUV < 26.5$, and a FUV flux limit of $FUV < 25$.

2.4. *Spectroscopic and Photometric Redshifts*

The DEEP2 redshift survey provides spectroscopic redshifts to $R_{\rm AB} < 24.1$ in AEGIS; see Davis et al. (2007) for details. Here we use only redshifts between $0.4 < z < 1.2$ with a confidence greater than 95% ($z_{\rm Quality} \geq 3$). With this quality cut, there are 2,885 galaxies with spectroscopic redshifts within the ACS region.

We additionally use photometric redshifts to both increase our sample size and allow us to probe fainter flux limits. We use CFHTLS T0003 release photometric redshifts from Ilbert et al. (2006), derived from *ugriz* imaging covering the central $1^\circ \times 1^\circ$ of the field. We remove from the sample all galaxies that are below our flux limit of $i_{AB} = 25$, that have large photometric errors, or that have a 5% or greater probability of being at a different redshift. We limit the sample to the redshift range $0.4 < z < 1.2$. At lower redshifts the volume probed is small, while the upper limit ensures that the ACS imaging samples rest-frame optical morphologies, thereby minimizing rest-frame wavelength-dependent morphology biases. Combined with DEEP2 redshifts, this results in a sample of galaxies with redshifts in the range $0.4 < z < 1.2$ with a median redshift of 0.75.

Using galaxies that have both DEEP2 spectroscopic and CFHTLS photometric redshifts, we are able to test the redshift precision of the photometric redshifts. Within the redshift range $0.4 < z_{spec} < 1.2$, there are 3,306 galaxies in both catalogs. Among these, 4.2% are catastrophic outliers, defined as having $|\Delta z|/(1 + z_{spec}) > 0.15$. Excluding catastrophic errors, the photometric redshifts have an accuracy of

$\sigma_{\Delta z/(1+z_{spec})} = 0.038$, with a normalized median absolute deviation: $\eta = 1.48$ and a median $[|\Delta z|/(1+z_{spec})] = 3.1\%$. See Ilbert et al. (2006) for a full discussion of the photometric redshifts.

Table 1 contains a summary of the datasets, sample sizes, and depths for the parent sample. The completeness of our parent sample depends on the detection limits of the ACS images and the completeness of the DEEP2 and CFHTLS redshift catalogs, which may depend on color and magnitude. The DEEP2 spectroscopic targeting selection excludes objects with a surface brightness fainter than $\mu_R \sim 26.5$ (Davis et al. 2007), whereas the CFHTLS photometric redshift catalog has no strong selection against low surface brightness objects as compared to the ACS detections (Lotz et al. 2008b). Due to the detection in DEEP2 spectra of emission lines in blue star-forming galaxies and absorption features in older, red galaxies and CFHTLS measurements of spectral breaks in all galaxy populations, the redshift catalogs are not strongly biased against galaxies with either red or blue colors (Lotz et al. 2008b). The dominate selection effect is due to the ACS detection limits of the morphology measurements. The ACS surface brightness detection limit of $\mu \sim 24.7$ results in the lowest surface brightness galaxies, which are likely to be blue, missing from the morphology catalog (Lotz et al. 2008b). For our statistical tests, we ensure to always match the stellar mass distributions of the different comparison samples, which minimized the selection effect of missing the lowest surface-brightness blue galaxies.

2.5. *K-Corrections and Stellar Masses*

We use the CFHTLS *ugriz* photometry and *GALEX* NUV/FUV magnitudes to calculate K-corrections (Blanton & Roweis 2007). We convert the observed fluxes to rest-frame absolute *GALEX* NUV and *UBVR* magnitudes in the Johnson-Morgan System.

We derive stellar masses for galaxies in our sample following Weiner et al. (2009), who show that reasonably robust stellar masses at these redshifts can be inferred from the rest-frame M_B and (U-B) colors, following color-M/L ratio relations (Bell & de Jong 2001). Comparing these stellar masses to those calculated by Salim et al. (2009), who fit spectral energy distributions (SEDs) for AEGIS galaxies using up to eight bands of photometry from the UV to the near-Infrared, we find a good agreement, with an offset of 0.13 dex and a scatter of 0.2 dex. The IMF used here and by Weiner et al. (2009) is a "Diet Salpeter" IMF (Bell et al. 2003).

3. GALAXY SAMPLE DEFINITIONS

We use rest-frame optical (U-B) colors to define our samples. As discussed below, we have tested that our results do not change if we instead use (NUV-R) colors, which more clearly separate star forming and quiescent galaxies. This shows that our results are robust against contamination in the green valley by dusty star forming galaxies. We define the rest-frame red, green, and blue galaxy color samples by first locating the magnitude-dependent minimum of the color bimodality. We use the well-defined magnitude-dependent slope derived using the red sequence and then solve for a color offset to locate the minimum of the green valley. To measure

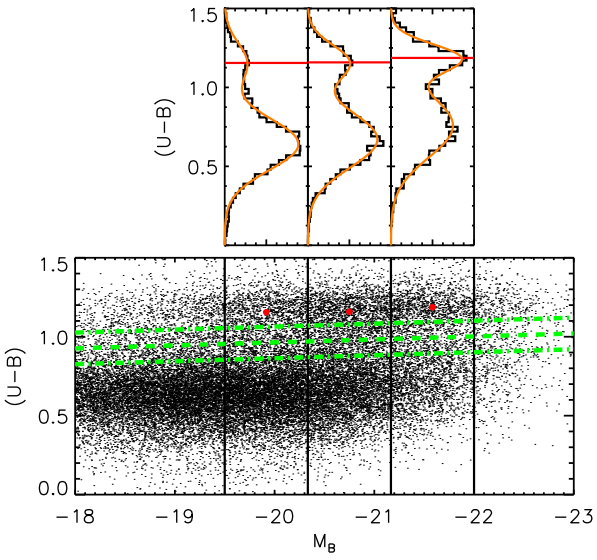

FIG. 2.— Color-magnitude diagram for AEGIS galaxies at $0.4 < z < 1.2$ and the definition of red, green, and blue galaxies. The upper panel shows double Gaussian fits (orange) to the (U-B) color distributions (black) for three magnitude bins between M_B =-19.5 and -23.0. We normalize the peak of the distribution in each magnitude bin to unity. We do not fit the magnitude-dependance of the red sequence below M_B=-19.5 or above M_B=-22 due to the lower numbers of red galaxies. The red lines show the peaks of the fit, used to fit a linear magnitude-dependent slope to the red sequence. This same slope is used to define the center of the green valley. The lower panel shows the color-magnitude diagram for galaxies with $0.4 < z < 1.2$. Red points mark the locations of the peak of the red sequence for each magnitude bin, and the green dashed lines show the center and width of the green valley as defined by Equation 1.

the slope of the red sequence, we fit a double Gaussian to the observed (U-B) color distribution in three magnitude bins (shown in the upper panel of Fig 2) and fit a linear color-magnitude relation to the maximum of the Gaussian fit to the red galaxies (shown as red dots in the lower panel of Figure 2). We then fit for an offset of this line to match the minimum in the observed color-magnitude diagram. The resulting definition of the center of the green valley is

$$(U-B) = -0.0189(M_B + 19.79) + 0.96 \qquad (1)$$

where the AB magnitude offset is given at the median of the parent sample.

We define the green valley to have a width of $\delta(U-B) = 0.1$ about the minimum line, with red galaxies having redder colors and blue galaxies having bluer colors. The width of the green valley is relatively arbitrary when using optical colors; our choice follows Coil et al. (2008). See the dot-dashed lines in Figure 2 for the color sample definition. From our parent sample of 2,437 galaxies, with this color-magnitude cut there is a total of 571 red, 342 green, and 1,524 blue galaxies. The color-magnitude cut used to separate blue and red galaxies in Willmer et al. (2006) for the DEEP2 sample is very similar to the cut used here. We do not allow the definition of the center of the green valley to evolve with redshift; however if a redshift evolution of ~ 0.1 per unit red-

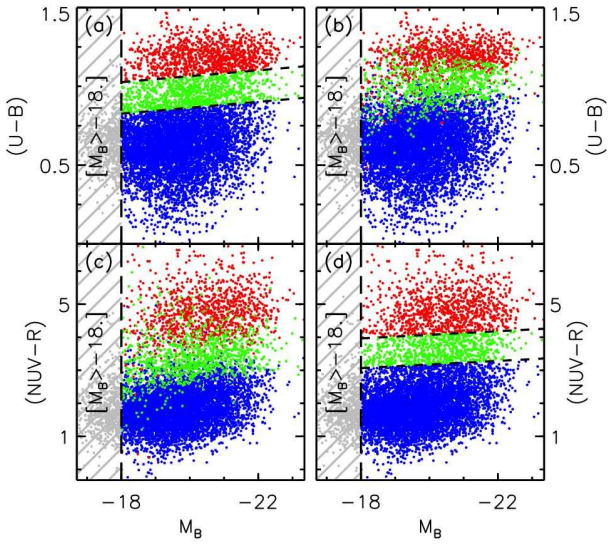

FIG. 3.— Comparison of green valley sample selection in different color-magnitude spaces. (a) Upper left panel: Rest-frame (U-B) color versus M_B magnitude. Green valley galaxies are defined in this space using a tilted color cut (see Equation 1). This is the sample definition used throughout the paper. We define the green valley to be within δ(U-B)=0.1 of the minimum of the (U-B) color bimodality. Galaxies are color-coded here by whether they are defined to be red, green, or blue in this space. (c) Lower left panel: Rest-frame (NUV-R) versus M_B for the same galaxies, color-coded by their definition in the panel above. (d) Lower right panel: We present an alternative definition of green valley galaxies using the observed bimodality in rest-frame (NUV-R) versus M_B space. Galaxies here are color-coded by their definition in this space (see text for details). (b) Upper right panel: The same galaxies, color-coded by their definition in the panel below, are shown here in rest-frame (U-B) versus M_B space. This figure shows that the selection of green valley galaxies at $0.4 < z < 1.2$ is very similar using either (U-B) or (NUV-R) colors.

shift (Blanton 2006) is included in our color-magnitude cut, none of our results or conclusions change.We do not create strictly volume-limited samples, as we are not attempting to measure evolution in the morphological parameters of green galaxies with redshift. We impose an absolute magnitude limit of $M_B > -18$, to ensure that our colors samples (red, green and blue) are of roughly similar depth. We show in Section 5.2 that the distribution of morphological parameters is not a strong function of magnitude near the limit used here.

We test the robustness of our results to the color used to define the green valley. In Figure 3 we show in the left panels samples defined using (U-B) colors (in (U-B)-M_B space in the top panel and in (NUV-R)-M_B space in the bottom panel), along with samples defined using (NUV-R) colors in the right panels (again with (U-B)-M_B in the top panel and (NUV-R)-M_B in the bottom panel). To define the green valley in (NUV-R)-M_B space, we fit for the M_B magnitude slope evolution by fitting a Gaussian to the blue galaxies in four bins in magnitude. The color-magnitude cut is then shifted to the center between the red and blue peaks. The width of the green valley in (NUV-R) color is defined as $\delta(NUV - R) < 0.45$, which is chosen to ensure that a similar fraction of galaxies in the full sample is defined to be green in either (U-B) or (NUV-R) space.

We find that galaxies defined to be in the green valley in (NUV-R) color also lie in or near the green valley as defined in (U-B) color, with some scatter. Galaxies that are defined to be green in one color that are *not* green in the other color still lie very close to the defined green valley. We have verified that performing all of the analyses in this paper with an (NUV-R)-selected sample does not change any of our results.

We note that the definition of the green valley in (NUV-R) color fit for and used here is bluer than the definition in Salim et al. (2009), who defined green galaxies as having $3.5 < (NUV - R) < 4.5$. Here our final green galaxy sample (defined in (U-B)-M_B space) lies within $3.2 < (NUV - R) < 4.1$.

4. MEASURED MORPHOLOGY PARAMETERS

We derive quantitative morphological parameters for all galaxies in our sample from the *HST*/ACS imaging. To sample rest-frame B-band morphologies across the redshift range $0.4 < z < 1.2$, we use observed V-band morphologies for galaxies with $z < 0.6$ and observed I-band morphologies for galaxies with $z \geq 0.6$. Morphological classifications are flux limited to $I_{AB} < 25$. Following Lotz, Primack, & Madau (2004) and Lotz et al. (2006), we measure morphologies for those objects that have large enough sizes (Petrosian radius $r_p \geq 0.3''$) and high enough signal-to-noise (mean S/N per galaxy pixel > 4 within the segmentation map) to yield robust morphological parameter measurements. The ¡S/N¿ threshold depends on the pixel scale, while the Petrosian radius threshold depends on both the pixel scale and the point spread function; therefore these thresholds are *HST*/ACS specific. The Petrosian radius r_p is defined as the semi-major axis length at which the ratio of the surface brightness at r_p to the mean surface brightness within r_p is equal to 0.2. r_p is computed within an elliptical aperture using the ellipticity computed from the SExtractor galaxy photometry software (Bertin & Arnouts 1996). The flux and radius cuts corresponds to an average surface brightness within the Petrosian radius of $\mu \sim 24.4$ AB magnitudes per square-arcsec (Lotz et al. 2008b). All of the quantitative morphological measurements below use the same segmented maps created by Lotz, Primack, & Madau (2004). With these cuts, our sample contains 2,437 galaxies with measured morphologies and redshifts within $0.4 < z < 1.2$. We derive a variety of morphological parameters; details of each are given below.

4.1. *CAS Parameters*

We define concentration (C), asymmetry (A), and smoothness (S) following Conselice (2003). The concentration parameter, which measures the central concentration of light in a galaxy (Bershady, Jangren, & Conselice 2000), is defined as

$$C = 5 \log \left(\frac{r_{80}}{r_{20}} \right) \quad (2)$$

where r_{80} and r_{20} are the radii that contain 80% and 20% of the total light, respectively. Elliptical galaxies are generally the most concentrated with $C \sim 4.5$,

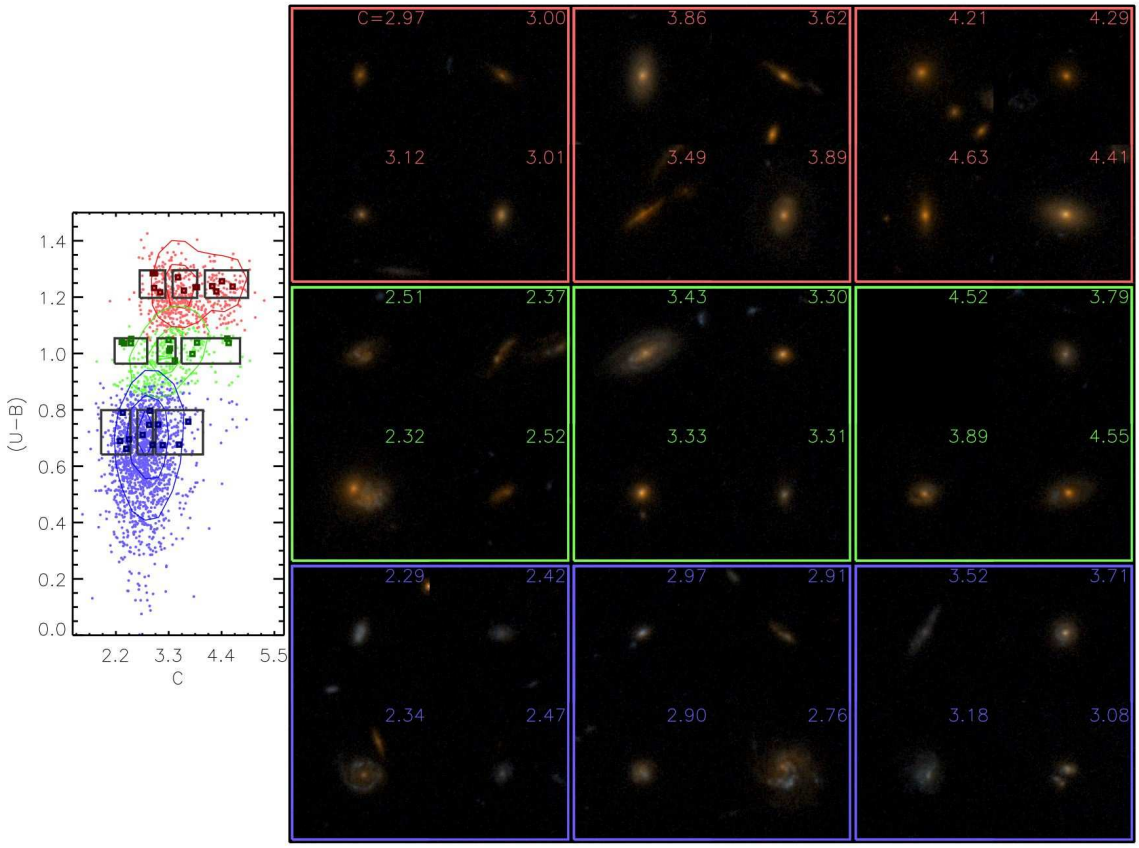

FIG. 4.— To help visualize the different morphology parameters that we include in this paper, we show here and in Figures 5 and 6 a random selection of *HST*/ACS $V + I$ color image postage stamps spanning the full range of the concentration, asymmetry, and B/T parameter for galaxies in each red, green and blue color space. To select the galaxies, each color space is divided into three areas, comprising the lower 20% extreme of the cumulative relevant morphological distribution, middle 30% centered at the median, and higher 20% extreme. The selection boxes are shown in the bivariate parameter and color plots to the left. Contours contain 30%, 50% and 80% of the individual color-parameter distributions. From within each selection region we randomly draw four galaxies; postage stamps for each are shown on the right, with the value of the measured morphology parameter shown in the top right corner of each postage stamp for that galaxy. Postage stamps are 6″ across, corresponding to ~ 65 kpc at $z = 0.8$.

and concentration is found to decrease with later Hubble types to $C \sim 2.5$ (Conselice 2003). In Figure 4, we show *HST*/ACS postage stamps (6″ on a side) of randomly-selected red, green and blue galaxies with relatively low, medium, and high concentration values within each color-selected sample. The left panel shows where the randomly-selected galaxies lie in color-concentration space, relative to the entire sample; the grey boxes show the regions used to select the galaxies with different concentration values. The concentration values for each galaxy shown are given in the upper right corner of each postage stamp.

Asymmetry is defined as the absolute value of the difference between the pixel intensities of a galaxy before ($I(i,j)$) and after a rotated by 180° about its center ($I_{180}(i,j)$), normalized by the integrated intensity:

$$A = \frac{\Sigma_{i,j} \| I(i,j) - I_{180}(i,j) \|}{\Sigma_{i,j} \| I(i,j) \|} - B_{180} \qquad (3)$$

Here a correction is made to subtract off the averaged asymmetry of the background near the galaxy (B_{180}). (see Conselice, Bershady, & Jangren 2000, for details). Asymmetry can be caused by spiral arms, dust lanes, mergers, or interactions, and is lowest with smooth elliptical light profiles and rises in star-forming and irregular galaxies, as well as on-going mergers (Abraham et al. 1994). Major mergers typically have $A \geq 0.35$, while spirals have $A \sim 0.25$ and elliptical galaxies have $A \sim 0.02$ (Conselice 2003). Similar to Figure 4, in Figure 5 we show postage stamps for randomly-selected galaxies with different asymmetry values within the red, green, and blue galaxy populations.

Smoothness is defined as the absolute value of the difference between the galaxy intensity pixel values ($I(i,j)$) and boxcar-smoothed intensity pixel values ($I_S(i,j)$) within $1.5 \times r_p$ of the center of the galaxy:

$$S = \frac{\Sigma_{i,j} \| I(i,j) - I_S(i,j) \|}{\Sigma_{i,j} \| I(i,j) \|} - B_S. \qquad (4)$$

Here again the average smoothness of the background (B_S) is removed. Low S values correspond to smoother light profiles, while high S values correspond to less smooth light profiles. The smoothness parameter is sensitive to higher frequency clumps that are differentiated from the smoother parts of the galaxy. Smoothness cor-

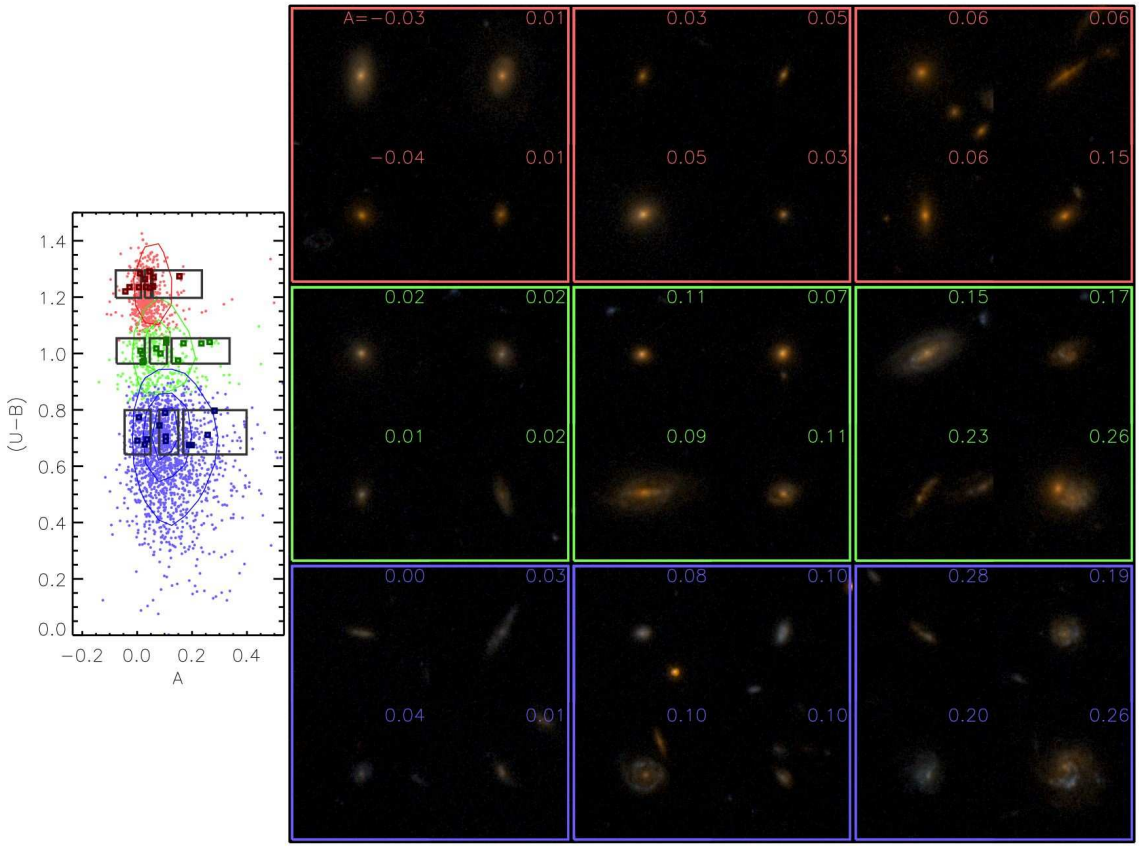

FIG. 5.— A random selection of *HST* postage stamps for galaxies spanning the measured asymmetry parameter (See Figure 4 for details).

relates with patchiness, which can be due to recent star formation or compact star clusters (Takamiya 1999). An important issue with smoothness is its dependence on the apparent size of a galaxy and the smoothing length ($0.25 \times r_p$), which can cause smaller galaxies to have smoothness values below the average smoothness of the background. This systematic issue with the smoothness parameter can limit its usefulness as a comparison parameter.

4.2. *B/T: Bulge-to-Total Decomposition*

Using two-dimensional bulge plus disk surface brightness profile models, we measure the bulge-to-total light fractions (B/T) using GIM2D (Simard et al. 2002). The B/T parameter provides a rough measure of how disk-dominated or bulge-dominated a galaxy is. The B/T parameter is estimated using a Sérsic profile, with the Sérsic index (n) defined in Sersic (1968), which controls the degree of curvature of the profile: a smaller n reflects a less centrally concentrated profile with a steeper slope at large radii. Often standard B/T fits at low redshift use a classical de Vaucouleurs profile with a Sérsic index of $n = 4$ fit to the bulge component. Here we use $n = 2$ to fit our higher redshift, younger galaxies, as many may not yet have formed a classical $n = 4$ bulge component. While using $n = 2$ or $n = 4$ can change the exact value of B/T measured for a given galaxy, it does not change the trends or conclusions we find here. The only significant difference is that in Table 3 we find a statistically different distribution between green and purple galaxies at the 5% level (see Section 6.5 for details). To be conservative, we adopt $n = 2$ here.

From the GIM2D V- and I-band best-fit model magnitudes of the entire galaxy (I_{galaxy}, V_{galaxy}) and bulge (I_{bulge}, V_{bulge}), the bulge-to-total fraction is defined as:

$$B/T = \begin{cases} 10.0^{(V_{galaxy}-V_{bulge})/2.5} & \text{for } z < 0.6 \\ 10.0^{(I_{galaxy}-I_{bulge})/2.5} & \text{for } z \geq 0.6 \end{cases}$$

Figure 6 shows postage stamps for red, green, and blue galaxies with a range of B/T parameters, similar to Figures 4-5.

4.3. *G: Gini Coefficient / M_{20}: Second-Order Moment of the 20% of light.*

In addition to the *CAS* and B/T morphological parameters, we also measure G/M_{20} (Lotz, Primack, & Madau 2004). The Gini coefficient (G) quantifies the distribution of light among the pixels in a galaxy and is defined as the absolute value of the difference between the integrated cumulative distribution of galaxy intensities and a uniform intensity distribution (Abraham, van den Bergh, & Nair 2003):

$$G = \frac{\Sigma_i^n (2i - n - 1)|X_i|}{|\bar{X}|n(n-1)} \quad (5)$$

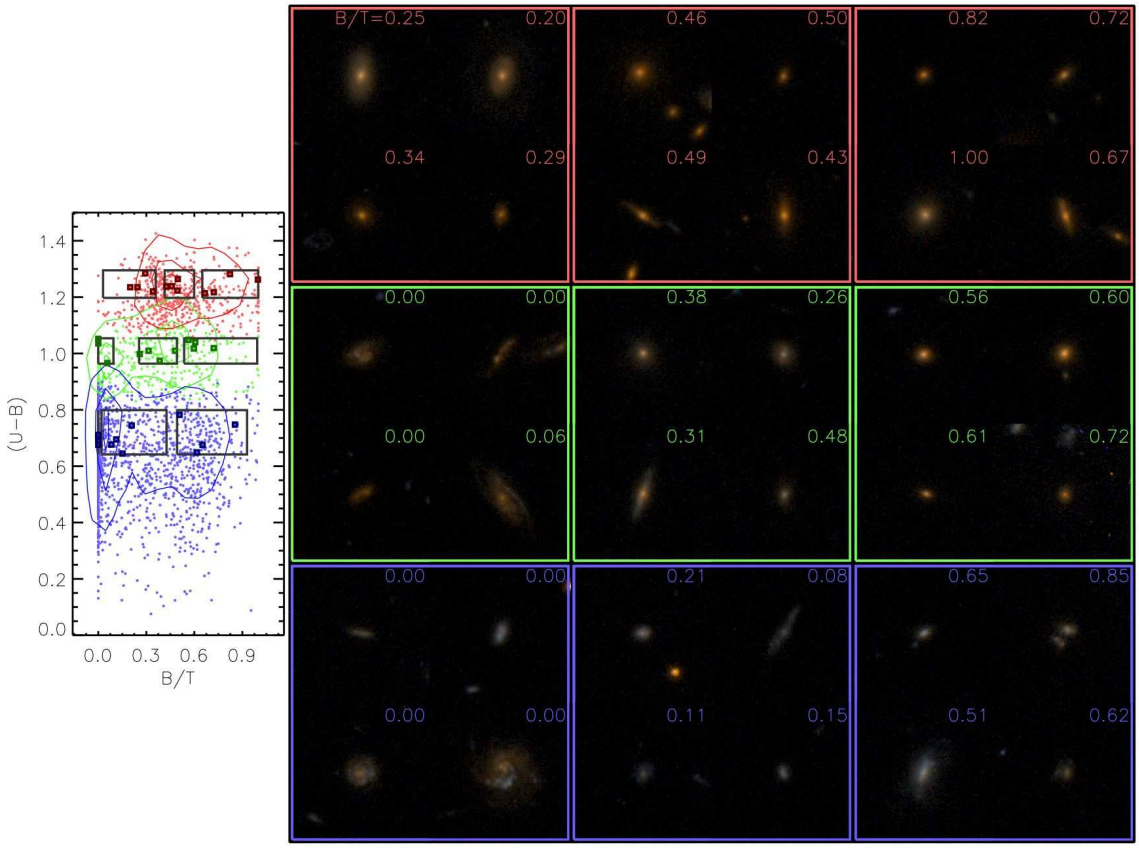

FIG. 6.— A random selection of *HST* postage stamps for galaxies spanning the measured B/T parameter (See Figure 4 for details).

where n is the number of pixels, X_i are the increasing ordered pixel flux values, and $\bar{X}$ is the mean pixel flux over the galaxy. G is close to unity if a single pixel contains all of the intensity and close to zero if the pixel values are uniform across the entire galaxy. G correlates with concentration and surface brightness, but it is not sensitive to the *location* of the brightest pixels. Therefore G is high for galaxies with multiple bright nuclei as well as centrally concentrated spheroids.

M_{20} is the second order moment of the brightest 20% of the galaxy light distribution, defined as the sum of the intensity of each pixel multiplied by the square of the distance from the center of the galaxy for the brightest 20% of the pixels in a galaxy. As such we can define M_{20} as:

$$M_{tot} = \Sigma_i^n f_i[(x_i - x_c)^2 + (y_i - y_c)^2] \quad (6)$$

$$M_{20} = \log\left(\frac{\Sigma_i M_i}{M_{tot}}\right), \quad \text{with} \quad \Sigma_i f_i < 0.20\ f_{tot} \quad (7)$$

where f_i are pixel fluxes and $(x_c,\ y_c)$ is the location of the galaxy center that minimizes the total second order galaxy moment, M_{tot}. M_{20} therefore traces the spatial extent of the brightest pixels and is anti-correlated with concentration.M_{20} is typically ~ -1.5 for late-type galaxies and ~ -2 for early-type galaxies (Lotz, Primack, & Madau 2004).

5. GREEN GALAXY MORPHOLOGIES

We first study various individual and joint distributions of both the general properties of green galaxies and their morphological properties, and compare them to the distributions of red and blue galaxies. The goal of this section is to understand the properties of galaxies in the green valley and how they differ from both red and blue galaxies.

5.1. *Galaxy Properties*

Figure 7 shows the general properties of red, green, and blue galaxies in the joint spaces of absolute B-band magnitude M_B, rest-frame (U-B) color, stellar mass, and Petrosian radius (r_p), which we use to estimate the size of the galaxy. Along the diagonal in this figure are individual parameter histograms for each color-selected sample, while off-diagonal panels show bivariate joint distributions.

The green galaxy sample has both an absolute magnitude M_B and stellar mass distribution that is intermediate between the red and blue galaxy samples. This is not surprising given the dependence of stellar mass on both color and magnitude. The median stellar mass of the red, green, and blue galaxy samples are fairly different, at 10.7, 10.3, and 9.6 log $M_*/M_\odot$, respectively. In addition, there is a well-known strong correlation between size, magnitude, and stellar mass, in

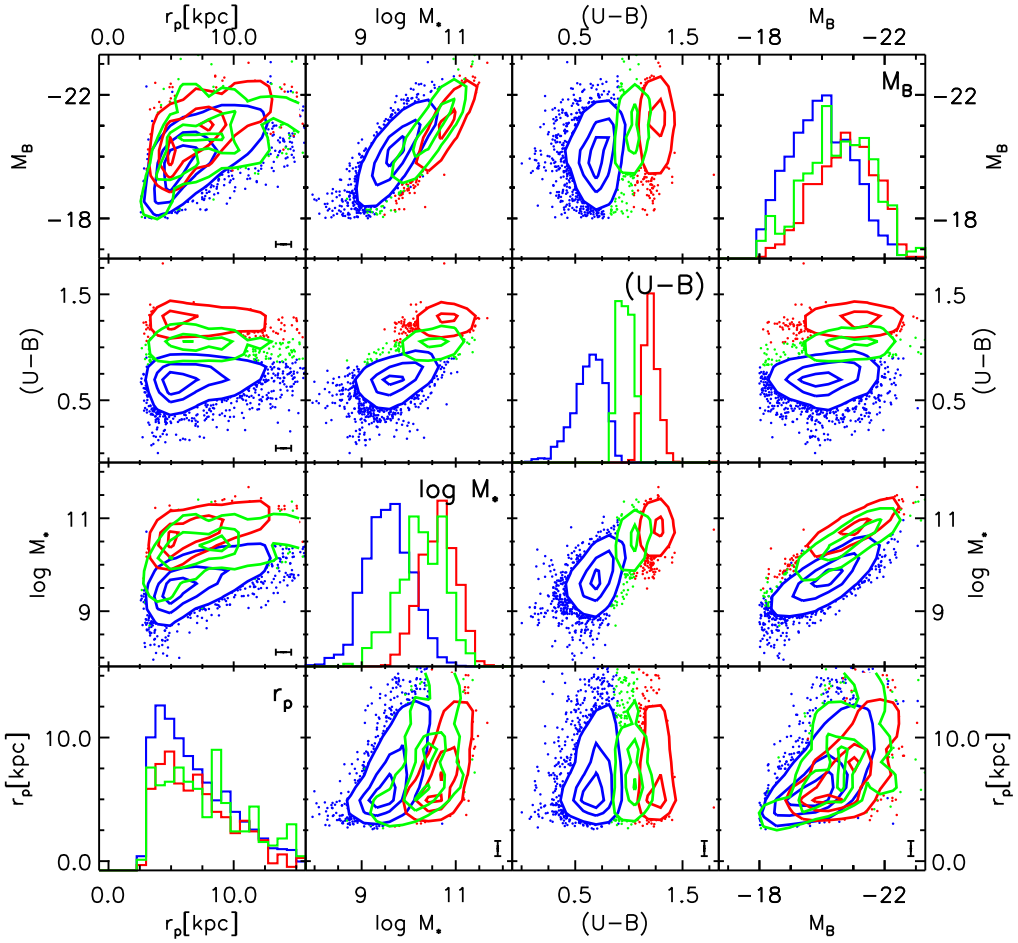

FIG. 7.— General properties of the AEGIS galaxy sample used here in the joint space of absolute B-band magnitude M_B, rest-frame (U-B) color, stellar mass, and Petrosian radius (r_p in units of kpc). Along the diagonal are individual parameter histograms for each color-selected sample, where we have weighted the red and blue galaxy histograms by a half and a quarter, respectively, to facilitate comparison with the green galaxies. Off diagonal panels show bivariate joint distributions, with contours containing 30%, 50%, and 80% of the sample; galaxies outside the 80% contour are shown as individual points. Contours have been smoothed using a Gaussian $1/20^{\rm th}$ of the size of the panel. The innermost 30% contour is not plotted if it is smaller than the grid used to calculate the contours. 1σ error bars at the median S/N pixel^{-1} of the sample, estimated from Lotz et al. (2006), are shown in the lower right corner of each space where available.

that brighter and/or more massive galaxies have larger sizes (Blanton & Moustakas 2009). However there is not a strong correlation between (U-B) color and Petrosian radius, except within the blue population. The green galaxy population on the whole has similar size and magnitude distributions to red galaxies. We note that the green galaxy sample has a tail to larger Petrosian radii than either the blue or red galaxy samples. Interestingly, Salim & Rich (2010) find using *HST*/ACS imaging that UV-excess, early-type galaxies that fall mainly in the green valley at low redshift are, on average, larger than either red or blue galaxies. We discuss the statistical significance of this result in Section 6.5. In Section 6.1, we will address possible stellar mass-dependent morphological differences between these samples by comparing samples with similar stellar mass distributions.

5.2. *CAS and B/T Parameter Results*

We next study the morphological distributions of green galaxies in CAS and B/T space and compare them with samples of red and blue galaxies. Figure 8 shows the distribution of red, green, and blue galaxies in terms of CAS, B/T, stellar mass, and (U-B) color with error bars, contours, and histograms similar to Figure 7. Error bars on morphological parameters are estimated from Lotz et al. (2006). We begin by investigating the individual parameter space distributions along the diagonal in Figure 8.

In terms of the concentration parameter, blue galaxies have $C \sim 2-3.5$, while red galaxies have $C \sim 3-5$. Green galaxies have an intermediate distribution, with $C \sim 2.5-4$. Unlike red galaxies, the green galaxy population does *not* contain a large fraction of galaxies with particularly high concentration values; 10% of green galaxies have $C > 4$ compared to 26% of red galaxies.

The fraction of galaxies with high asymmetry is dependent on color. Blue galaxies have larger asymmetry val-

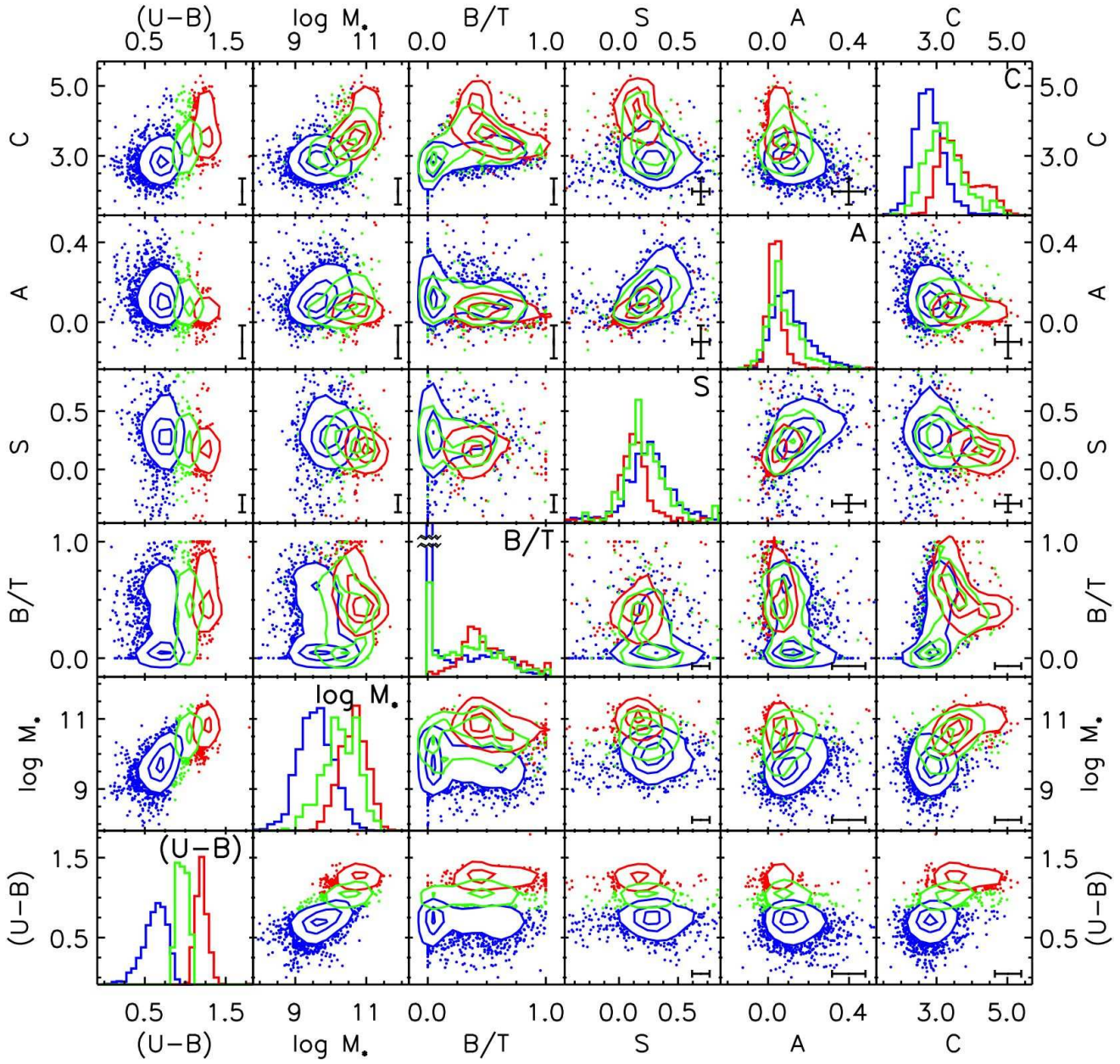

FIG. 8.— Morphological properties of red, green, and blue galaxies at $0.4 < z < 1.2$ in AEGIS. Shown are joint distributions of galaxy rest-frame (U-B) color, stellar mass, concentration (C), asymmetry (A), smoothness (S), and bulge-to-total light fraction (B/T). Along the diagonal are distributions for each individual parameter, where the red, and blue distributions have been scaled down by a factor of two, and four, respectively. Due to the large fraction of bulge-less ($B/T = 0$) blue galaxies, we limit the range of B/T to be 50% of the full range. The bivariate parameter distributions have contours plotted at 30%, 50%, and 80% of the total sample. The innermost 30% contour is not plotted if it is smaller than the grid used to calculate the contours. 1σ error bars at the median S/N pixel^{-1} of the sample, estimated from Lotz et al. (2006), are shown in the lower right corner of each space where available.

ues than red galaxies on the whole. Using the threshold of $A > 0.35$ that is typically used to define mergers, for example, we find that 3% of blue galaxies and 0.4% of red galaxies have $A > 0.35$. Using a threshold of $A > 0.2$, which clearly separates the tail of the distribution, we find that 17% of blue galaxies and 1.2% of red galaxies have $A > 0.2$. The green galaxy population has a similar asymmetry distribution as the blue galaxy population, though fewer green galaxies have large A values (1.2% have $A > 0.35$ and 8% have $A > 0.2$). Using either high A threshold, we find a lower percentage of highly asymmetric green galaxies compared to blue galaxies. This implies that while green galaxies have similar amounts of asymmetry as blue galaxies due to star formation knots, dust lanes, and/or spiral arms, they do not have as high a fraction of major mergers as the blue galaxy population (see Section 5.3 for a discussion of the merger fraction in each population using G-M_{20}).

To determine robustly the smoothness parameter of a galaxy one requires a larger threshold in spatial extent than for measuring concentration or asymmetry. The threshold required for smoothness is $r_p \geq 0.6''$, compared to $r_p \geq 0.3''$ required for concentration and asymmetry. Therefore smoothness can be measured for only roughly half of the galaxies in our sample. We find that red galaxies have lower S values than blue galaxies, on the whole, which reflects the fact that red galaxies generally have smoother light profiles. The green galaxy population has a somewhat similar S distribution as the blue galaxy population, though with more galaxies having lower S values. The median S values of red, green, and blue samples are 0.12, 0.19, and 0.24, respectively.

Continuing down the diagonal of Figure 8 to the B/T parameter, we find that while blue galaxies have a range of B/T values from 0 to ~ 0.8, a large fraction (30%) have $B/T = 0$, implying a disk-only galaxy with no bulge component. In Figure 8, the smallest B/T bin contains that 44% of blue galaxies with $0 \leq B/T < 0.05$. By-eye inspection of the *HST*/ACS images of these bulge-less galaxies confirms that these are disk-only systems. Due to this enhancement at $B/T = 0$ for the blue population, we limit the y-axis on the histogram plot of B/T to 50% of the peak number of blue galaxies at $B/T = 0$ to clearly show the full distribution of each color sample. Red galaxies have larger B/T fractions than blue galaxies, on the whole, with a distribution centered at $B/T \sim 0.4$, and very few bulge-less galaxies (0.9%, 1.5% with $0 \leq B/T < 0.05$). Green galaxies have a B/T distribution that is similar to blue galaxies, though with a smaller fraction (12%, 21% with $0 \leq B/T < 0.05$) of bulge-less galaxies. Figure 6 includes *HST*/ACS postage stamps of four randomly-selected bulge-less green galaxies in the central left sub-panel.

These bulge-less green galaxies are particularly interesting as the creation mechanism for these galaxies is unclear. We have visually inspected the *HST*/ACS images of these sources to check that they indeed have no apparent bulge component and are disk-only systems. We further investigate whether this population is dominated by dusty star-forming galaxies. In the (NUV-R) versus SSFR space shown in Figure 13, these bulge-less green galaxies (outlined by black diamonds) span the entire green galaxy population. We find that there is not a statistically significant difference in the dusty fraction

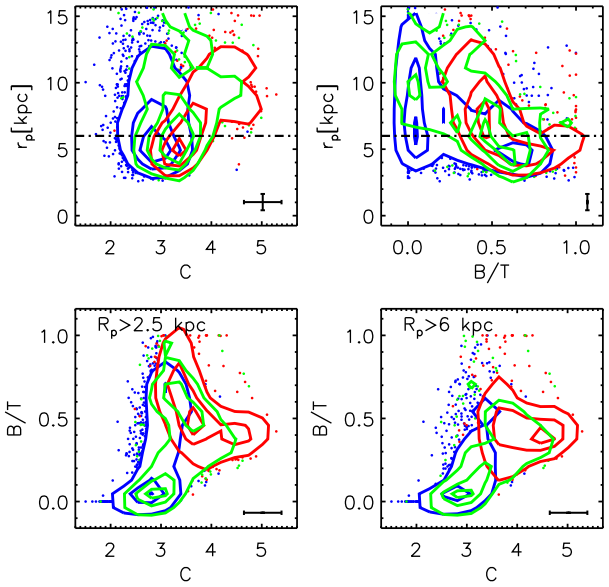

FIG. 9.— An investigation of how the measured C and B/T parameters depend on galaxy size. The upper panels show the measured Petrosian radius (r_p) as a function of C and B/T for our red, green, and blue galaxy samples. The dashed line at $r_p = 6$ kpc shows the threshold used in the lower right panel. Contours and error bars are similar to Figure 8. The lower left panel shows B/T versus C for all galaxies with $r_p > 2.5$ kpc. Both green and red galaxies show an odd trend of low C and high B/T. In the lower right panel only galaxies with $r_p > 6$ kpc are included and this trend disappears.

of green galaxies with $B/T = 0$ ($27 \pm 5\%$) compared to the entire green galaxy population ($21 \pm 3\%$). Therefore the bulk of this population should be transition objects from the blue cloud to the red sequence. As these galaxies do not have a bulge, it is unlikely that they have central AGNs which could lead to strong feedback. It is also unlikely that they have had many major mergers, which presumably would have led to the creation of a bulge component. The existence of these bulge-less green galaxies therefore places strong constraints on the quenching mechanism(s) at work in this population.

In addition to the individual parameter distributions shown in Figure 8, we can study the bivariate distributions between various morphological parameters. In C-A, A-S, and C-S space, in general green galaxies are an intermediate population between red and blue galaxies. The greatest differences between green galaxies compared to red and blue galaxies are seen in concentration and to a lesser extent in asymmetry. In Section 6.5 we discuss the statistical significance of these differences since they may provide insight into the underlying physical mechanism(s) that shut off star formation in galaxies.

There are interesting differences between the galaxy populations in the B/T-C parameter space. Within the blue galaxy population there is very little correlation between B/T and C, except that the bulge-less ($B/T = 0$) galaxies have the lowest concentration. However, within the red galaxy population there is an odd correlation in that the galaxies with the highest B/T values have the lowest concentration values. This is likely not real

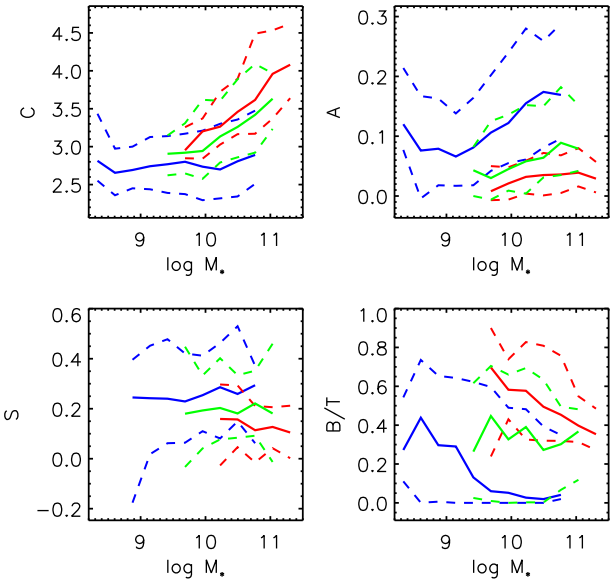

FIG. 10.— Conditional distribution plots which show the median and 68% range for the red, green and blue galaxies. The four subplot show concentration, asymmetry, smoothness, and bulge to total fraction values at a given mass. For a fixed stellar mass Green galaxies have higher concentration, and lower asymmetry values as compared to the blue galaxies.

but is due to these red galaxies with low C and high B/T values being very compact, such that C is not well-measured. Comparing C with r_p for each color sample (see Figure 9) we find that within the blue and green populations there is no correlation, but within the red population the galaxies with $r_p < 6$ kpc have small measured concentrations, with $C < 4$. These galaxies also have the highest B/T values, with $B/T > 0.7$. Keeping only galaxies with $r_p > 6$ kpc, we find that very few sources have $B/T > 0.6$ and within the red population there is no longer a correlation between B/T and C.

Green galaxies in the B/T-C space have a distribution that is more similar to blue galaxies than red galaxies, though there is a tail with high concentration, as seen in the red galaxy sample. For a given B/T value, green galaxies have higher concentrations than blue galaxies. This trend holds in the sample of galaxies with $r_p > 6$ kpc. We discuss the implications of this in Section 7.

Finally, in the M_*-C parameter space, we find that the red and blue galaxy populations lie in distinct regions of this space. The green galaxy population appears to span the red and blue distributions, possibly as a transition population moving from low stellar mass and low concentration (like the blue galaxies) to higher stellar mass and higher concentration (like the red galaxies).

In Figure 10 we highlight these differences by showing the C, A, S, and B/T morphological distributions (mean and 68% range) of each of the red, green, and blue galaxy samples as a function of stellar mass. This figure shows that at a given stellar mass green galaxies have larger C values, lower A values, and lower S values than blue galaxies. The B/T values may be higher than blue galaxies at a given stellar mass, but the noise in the mean and the similar width of the distributions make it difficult to draw a strong conclusion.

TABLE 2
RGB G/M_{20} MORPHOLOGICAL TYPES[a]

	Red	Green	Blue
Mergers	12 ± 2 %	14 ± 2 %	19 ± 1 %
Early Type	66 ± 5 %	35 ± 4 %	8 ± 1 %
Late Type	22 ± 2 %	51 ± 5 %	73 ± 3 %

[a] Percentage of each galaxy sample with $0.4 < z < 1.2$ classified into morphological types using G/M_{20}. Uncertainties include both Poisson error and uncertainties in the measured values of G/M_{20}. These fractions are measured over a wide redshift range in samples that are not volume-limited and thus should not be taken as the global fractions for red, green and blue galaxies. Please see Table 3 in Lotz et al. (2008b) for a the redshift-evolving fraction. These results here are shown to emphasize the relative fractions in our red, green, and blue galaxy samples.

5.3. *Rough Morphological types using G/M_{20}*

From the work of Lotz, Primack, & Madau (2004) and Lotz et al. (2008b), galaxies can be classified into rough morphological types: early, late or merger, depending on their location in G-M_{20} space (see Figure 11 for the cuts shown in the space). Following Lotz et al. (2008b), we define

$$\begin{aligned} \text{Mergers} &: G > -0.14M_{20} + 0.33, \\ \text{Early(E/S0/Sa)} &: G \leq -0.14M_{20} + 0.33, \text{ and} \\ &\quad G > 0.14M_{20} + 0.80, \\ \text{Late(Sb} - \text{Ir)} &: G \leq -0.14M_{20} + 0.33, \text{ and} \\ &\quad G \leq 0.14M_{20} + 0.80, \end{aligned}$$

in the G/M_{20} plane, which are based on visually determined morphologies in the EGS (Lotz et al. 2008b). Note that mergers in this plane include both major and minor mergers, whereas high asymmetry ($A > 0.35$) is only sensitive to major mergers (Lotz, Primack, & Madau 2004).

Table 2 contains the fraction of galaxies in the red, green, and blue galaxy populations used here that is classified as early type(E/S0/Sa), late type(Sb-dI), or merger. We derive errors on these fractions by performing Monte Carlo tests using the median errors estimated for G and M_{20} from the median S/N pixel^{-1} (Lotz et al. 2006). We also include in quadrature Poisson errors. Note that these fractions should not be interpreted as the fraction for all galaxies at these redshifts, as our samples are not strictly volume-limited and they cover a wide redshift range. We refer the reader to Table 3 in Lotz et al. (2008b) for the redshift-evolving morphological fraction of volume-limited color-defined galaxy samples at these redshifts. Here we use the derived fractions to compare relative trends between the different color-selected galaxy samples.

From Table 2 we find that the green galaxy population is intermediate between the red and blue galaxy populations in terms of each of the three morphological types. Compared to the green galaxy population, the blue population has a statistically higher merger fraction (2σ),

more late type galaxies (4σ), and fewer early type galaxies (7σ), while the red population has a lower merger fraction (1σ), fewer late type galaxies (5σ), and more early type galaxies (5σ). Comparing our results with the fractions found by (Lotz et al. 2008b), we find the same general trends, though we have somewhat higher merger fractions for all three galaxy samples.

5.4. *Rotated Gini and M_{20} Parameters*

We also analyze our samples in the G'/M'_{20} parameter spaces, which are plane rotated versions of G/M_{20}. These versions are created by rotating G/M_{20} such that the locus of galaxies, spanning from late to early types, now lie along the M'_{20} axis. The locus is roughly parallel to the merger definition line and is perpendicular to the late and early type definition line. In Figure 11, we plot red, green, and blue galaxies in G/M_{20} bivariate space in the top row, along with the corresponding rotated G'/M'_{20} space in the bottom row. 30%, 50% and 80% contours are plotted, along with the morphological classification lines, for both the standard and rotated spaces. This rotation will not effect the rough morphological types found in Table 2, but it breaks the degeneracy between the G and M_{20} parameters, such that the G' parameter reflects merger activity, while M'_{20} correlates with Sérsic index. The rotated variables are defined as

$$\begin{bmatrix} M'_{20} \\ G' \end{bmatrix} = \begin{bmatrix} \cos(\theta) & -\sin(\theta) \\ \sin(\theta) & \cos(\theta) \end{bmatrix} \times \begin{bmatrix} M_{20} \\ G \end{bmatrix}$$

with $\theta = 0.164$ radians fit from the locus of galaxies in the G/M_{20} plane.

Similar to Figure 8, in Figure 12 we consider the rotated G'/M'_{20} space and joint distributions with both stellar mass and (U-B) color. Contours, histograms, and error bars are similar to Figure 8.

In the one-dimensional G' space (upper right panel of Figure 12), the blue population contains a wider distribution that extends to both larger and smaller values of G' compared to the red galaxy population. As higher G' values correlate with merger activity (reflecting both major and minor mergers), this implies a larger merger fraction for blue galaxies compared to red galaxies. Small values of G' can result from very dusty galaxies. The green galaxy population has an intermediate distribution in G' between the blue and red galaxy distributions. In particular, the green galaxy population has a lower fraction of objects with high G' values compared to blue galaxies and a higher fraction than red galaxies. This implies a merger fraction that is lower than what is found for the blue galaxy population but higher than the red galaxy population.

Similar to the concentration parameter distribution, the green galaxy population is intermediate between the red and blue galaxies in the M'_{20} parameter space, where red galaxies have a higher mean value of M'_{20} than blue galaxies. There is a sharp distinction between the red and blue galaxy populations in M'_{20} which is more pronounced in M'_{20} compared to G'. While the green galaxy distribution spans the majority of both the red and blue populations, it does not include the highest values of M'_{20} seen in the red galaxy distribution or the lowest values seen in the blue galaxy distribution.

In the joint M'_{20}-G' space, differences between the red, green, and blue populations are more distinct in M'_{20} than G'. While there is very little correlation seen between stellar mass and G', there is a strong correlation between stellar mass and M'_{20}. As with stellar mass and concentration, here again the red and blue galaxy populations lie in distinct areas of M_*-M'_{20} space. The green galaxy population appears to be intermediate, although their distribution is more similar to red galaxies than blue galaxies. For a given stellar mass, green galaxies have lower M'_{20} values than red galaxies, and the green galaxy population on the whole has many fewer galaxies with low M'_{20}, as seen for the blue galaxy population.

5.5. *Environmental Dependence of the Color-Morphology Relation*

We further investigate the joint environment-stellar mass-morphology distribution of red, green, and blue galaxies by comparing the morphological distributions as a function of stellar mass of each galaxy color sample in different environments. Using the projected third-nearest-neighbor density catalogs of Cooper et al. (2006), we estimate the local environment or over density of each red, green, and blue galaxy in our sample. We find no significant difference in the morphology-stellar mass distribution of galaxies of a given color when split into roughly equal-sized populations in over- or under-dense regions. To compare the morphology-stellar mass distributions of galaxies in the most extreme environments within our sample, we select galaxies such that they have $|\log_{10}(1+\delta_3)| > 0.25$, and do not find any significant differences in the C, A or B/T parameters. We additionally use the DEEP2 group catalogs of Gerke et al. (2007) to identify galaxies likely to be in groups, with velocity dispersions $\sigma_v \geq 150$ km s^{-1} or in the field. We compare the morphology-stellar mass distributions of red, green, and blue galaxies in groups versus the field and find no significant differences, though we note that the errors are somewhat large due to small numbers of galaxies in each color-stellar mass-morphology-environment bin.

6. GREEN VERSUS PURPLE GALAXY COMPARISON

The second goal of this paper, beyond measuring the morphological distributions of green valley galaxies, is to quantitatively determine whether the green galaxy population can be explained from a morphological point of view as a simple mix of blue and red galaxies, or whether green galaxies have a distinct morphological make-up that defines them as a separate, distinct population. To undertake this second goal, we wish to compare the morphological distribution of green galaxies with the distribution of red and blue galaxies taken as a whole. However, we can not simply take the union of the red and blue galaxy samples used here to compare with the green galaxy sample, as the morphologies of the red and blue galaxy populations differ significantly. As a result, the morphological distribution of their union will depend on the ratio of red to blue galaxies in the combined sample. We therefore create "purple" galaxy comparison samples that have the same ratio of red to blue galaxies as within the green population itself. We also create comparison samples that have had dusty galaxies removed and have

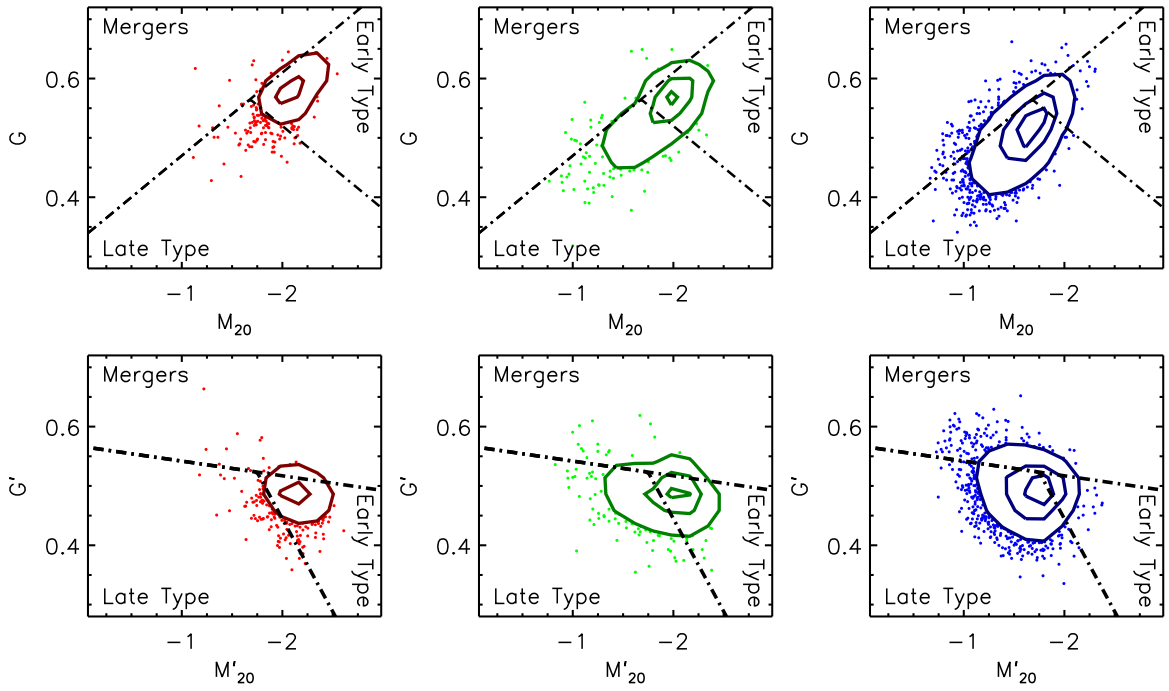

FIG. 11.— Using the cuts defined in Lotz, Primack, & Madau (2004), we divide the G/M_{20} space (top row) into areas with galaxies that are early-type (E/S0/Sa), late-type (Sb/Sc/Ir), or mergers and plot the locations of red, green, and blue galaxies. Contours and error bars are similar to Figure 8. The bottom row shows the same galaxy samples in a rotation version of this space in which the locus of galaxies lies along the G' axis (see text in Section 5.4 for details). Using this rotated definition, the M'_{20} axis relates more directly to the negative of the Sérsic index and G' correlates with merger identification. Due to the tight grouping of the red galaxy population in these spaces, the innermost 30% contour is not shown.

matched stellar mass distributions, to limit possible biases in our statistical tests.

We found in Section 5.1, when comparing red, green, and blue galaxies in various morphological parameter spaces that the green galaxy population appears to be intermediate between the red and blue galaxy populations. Using the purple comparison samples, we can test statistically if green galaxies are in a transition phase, moving from the blue cloud to the red sequence; however, these results could also potentially be consistent with green galaxies being a simple mix of the red and blue galaxy populations.

6.1. `Full` *"Purple" Galaxy Comparison Sample*

We first define a "purple" galaxy sample, which combines the red and blue galaxy populations to compare against the green galaxy population. Starting with the red and blue galaxy samples defined above, we weight the galaxies such that the combined sample has the same ratio of red to blue galaxies as galaxies in the green sample above and below the minimum in the color bimodality (the dashed line in Figure 2 defining the center of the green valley). In this way, the ratio of galaxies above and below the minimum in the color bimodality is the same for the green galaxy sample and the comparison "purple" galaxy sample. We refer to this sample as the 'full purple galaxy sample' (labeled `Full` in the figures below). The `Full` purple galaxy sample contains a total of 2,037 galaxies, weighted to an effective sample size of 487 galaxies, with a ratio of red to blue galaxies of 0.82.

6.2. *Removing Dust Obscured Galaxies*

While the optical color of galaxies reflects their star formation history and the age of their stellar populations, it can be influenced by the presence of dust. In particular, galaxies in the green and red populations may have older stellar populations than blue galaxies, or they may appear to be redder due to dust obscuration. As the goal of this paper is to study the morphologies of green galaxies as a potential transition population of galaxies that are moving from the blue cloud to the red sequence, we would like to identify and remove interlopers from the green and red populations that are dusty star forming galaxies.

Salim et al. (2009) show that a comparison between the SSFR versus rest-frame (NUV-R) color of $z \sim 1$ galaxies (their Fig. 6) indicates that while the bulk of green galaxies (defined in Salim et al. (2009) using (NUV-R) color) are transition objects with SSFRs intermediate between blue and red galaxies, a fraction of green galaxies are likely green due to dust in the host galaxy. These dusty green galaxies may therefore not be transition objects moving from the blue cloud to the red sequence. Following (Salim et al. 2009), we identify and remove these dusty 'interlopers' in our green and red galaxy samples. We use SSFR as derived in (Salim et al. 2009), who use stellar population synthesis models to fit nine bands of photometry for AEGIS galaxies (FUV, NUV, $ugriz$, K_s). Figure 13 shows SSFR versus (NUV-R) color for our optical color-selected galaxy samples. There is a relatively tight, well-defined

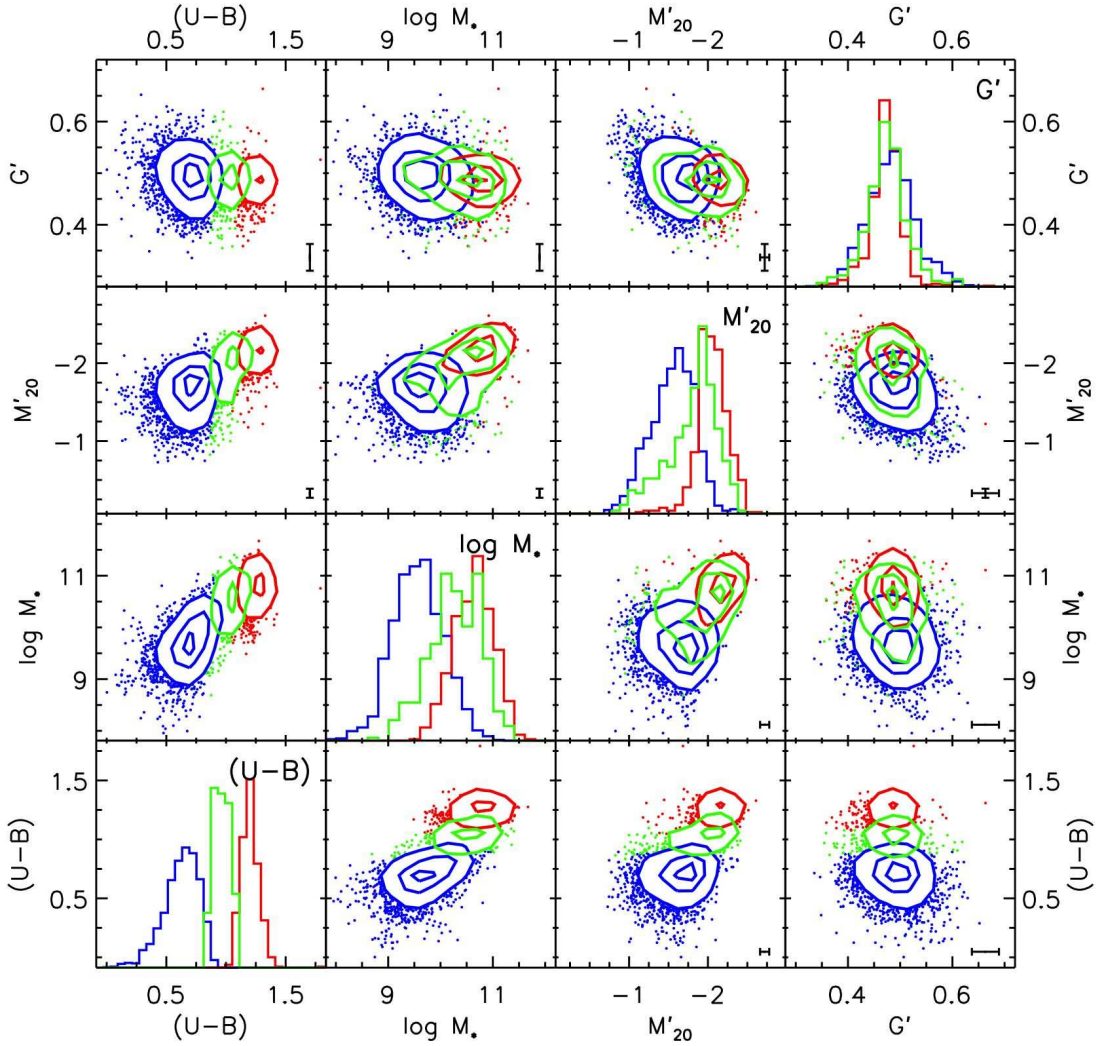

FIG. 12.— Measured G'/M'_{20}, stellar mass, and (U-B) color joint parameter spaces. Contours, histograms, and error bars are similar to Figure 8.

locus in this space, as indicated by the dot-dashed line. Galaxies that lie $\geq 3\sigma$ higher than this locus (in the upper right corner of Figure 13, above the dashed line) are likely to have optical colors affected by dust obscuration. We remove these galaxies from the green and red samples used here to create a "$\texttt{Full}_{\rm NUV}$ green sample" and a corresponding "$\texttt{Full}_{\rm NUV}$ purple sample" that has the same ratio of red to blue galaxies (0.83) as the "$\texttt{Full}_{\rm NUV}$ green galaxy" sample. All sample definitions denoted with subscript "NUV" have dusty obscured galaxies removed from the green and red populations. This procedure removes a total of 123(36%) green galaxies and 92(16%) red galaxies. The $\texttt{Full}_{\rm NUV}$ purple sample contains a total of 2003 galaxies, weighted to an effective sample size of 438 galaxies. The $\texttt{Full}_{\rm NUV}$ green sample contains 219 galaxies.

6.3. *Matched Stellar Mass Galaxy Samples*

Figure 14 shows the stellar mass distributions of the red, green, and blue galaxy samples (first panel), the `Full` green and purple samples (second panel), and the $\texttt{Full}_{\rm NUV}$ green and purple samples (third panel). As noted in Section 5.1, optical color and stellar mass are highly correlated. As a result, the green galaxy samples have higher stellar mass, on average, than the corresponding purple comparison samples. To remove any dependence of morphology on stellar mass when comparing the green and purple samples, we create a purple comparison sample that has the same stellar mass distribution as the green $\texttt{Full}_{\rm NUV}$ sample (shown in the right panel of Figure 14). To create this sample we assign weights to red and blue galaxies in the $\texttt{Full}_{\rm NUV}$ purple sample in bins of $\log(M_*/M_\odot) = 0.1$ such that the stellar mass in each bin matches that of the stellar mass distribution of green galaxies either above (for red galaxies) or below (for blue galaxies) the minimum of the green valley. By weighting the red and blue galaxies to the green galaxies above and

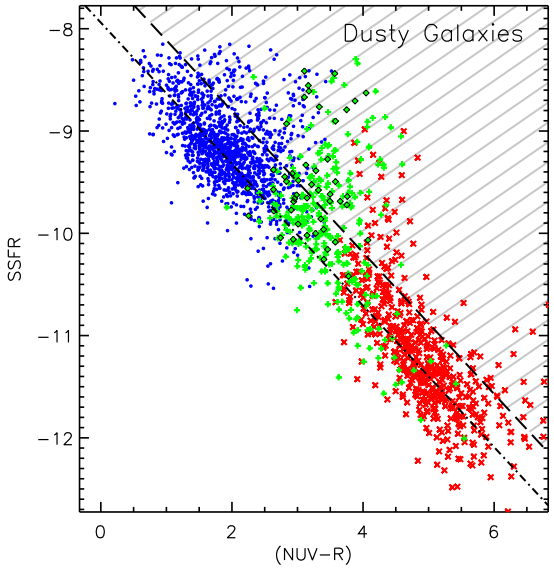

FIG. 13.— (NUV-R) color plotted versus specific star formation rate (SSFR) for the red, green, and blue galaxy samples used here. Galaxies with optical colors affected by dust will be scattered into the upper right corner of this plot, away from the main locus of galaxies (dot-dashed line). We identify and remove green and red dusty galaxies that lie more than 3σ (the dashed line) above this locus in our "NUV" samples. Green galaxies with $B/T = 0$ are shown outlined by black diamonds.

below the color minimum, we also constrain the ratio of red to blue galaxies to be the same as that within the green population (defined as above and below the minimum color that defines the center of the green valley) to within a few precent. The resulting `Stellar Mass`$_{\rm NUV}$ sample contains a total of 1970 purple galaxies weighted to an effective sample size of 217 galaxies, with a red to blue ratio of 0.82.

6.4. *"Purple" vs Green Galaxy Comparison*

In Figures 15-17 we plot distributions in CAS, B/T, and G'/M'_{20} for the red, green and blue (`RGB`) samples, alongside each of the green and purple comparison samples, `Full`, `Full`$_{\rm NUV}$, and `Stellar Mass`$_{\rm NUV}$, to examine differences in the bivariate distributions of the green and purple galaxy samples. Contour levels and error bars are similar to Figure 8.

In Figure 15 we compare the joint CAS distributions of green and purple galaxies and find that the same trends that exist for the `Full` samples persist after we both remove dusty interlopers and match the samples in `Stellar Mass` distribution. In concentration and asymmetry, we find a missing tail of high asymmetry ($A > 0.2$) and low concentration ($C < 3.0$) galaxies in the green samples, when compared to the purple samples. Additionally, the green galaxy population is also missing a tail of higher concentration galaxies ($C > 4.5$) seen in the purple samples. These trends are reflected in the distributions of $C - S$ and $A - S$, where the green population is found to lack galaxies at the highest and lowest concentrations, as well as high asymmetry.

In Figure 16 we show bivariate distributions of the green and purple comparison samples in the standard G/M_{20} space as well as in the rotated $G' - M'_{20}$ space.

TABLE 3
KOLMOGOROV-SMIRNOV TWO SAMPLE SIGNIFICANCE-LEVELS [a]

	Range	`Full`	`Full` $_{\rm NUV}$	`Stellar Mass`$_{\rm NUV}$
log M$_*$	[7.8, 12.2]	< 0.01%	< 0.01%	72%
C	[1.3, 5.7]	0.32%	0.16%	0.73%
A	[-0.2, 0.5]	80%	52%	3.5%
S	[-0.5, 0.9]	55%	66%	77%
B/T	[-0.2, 1.2]	2.6%	12%	4.3%
M_{20}	[-0.1, -3.0]	7.5%	0.39%	2.0%
G	[0.3, 0.7]	43%	72%	25%
M'_{20}	[-0.1, -3.0]	7.3%	0.41%	1.9%
G'	[0.3, 0.7]	70%	69%	99%
r_p[kpc]	[-0.8, 15.8]	0.34%	55%	32%

[a] KS test significance levels for each green and purple comparison sample. Parameters that can be rejected as being drawn from the same parent population at the 5% and 1% significance levels are highlighted with light grey and dark grey backgrounds, respectively.

We find that the green galaxy samples do not span the entire locus seen for the purple samples. In particular, the green galaxy samples do not contain objects with the lowest G or M_{20} values seen in the purple sample. This difference is particular clear in the `Stellar Mass`$_{\rm NUV}$ sample comparison. These differences are also seen in the rotated G'/M'_{20} plane. We also compare the G' and asymmetry distributions, as both parameters are sensitive to mergers. Asymmetry is a tracer of major mergers, while G' tracers both major and minor mergers (Lotz et al. 2010). We find that the green and purple samples have similar distributions in $G' - A$. The `Stellar Mass`$_{\rm NUV}$ samples show a tail of galaxies to high A values that is not seen in the green sample (as seen in Figure 15 above).

We note that in Figures 15-17 there are only minor differences between the `Full`, `Full`$_{\rm NUV}$, and `Stellar Mass`$_{\rm NUV}$ samples, indicating that our results are not dominated by effects due to dust obscuration or the stellar mass-dependence of the green and purple galaxy samples.

In Figure 17 we compare the distribution of B/T with C, A, and S for the green and purple samples. Here we find that the green galaxy population does not contain as many galaxies at high B/T as the purple population, in addition to lacking galaxies at the highest asymmetry and smoothness values.

6.5. *Morphological Parameter Distribution Tests*

For each of the measured morphological parameters, we apply the two-sided Kolmogorov-Smirnov (KS) statistic as a nonparametric null hypothesis test of the difference between the green and purple comparison samples. The null hypothesis is that both populations are drawn from the same parent sample. The KS statistic measures the maximal difference between the two normalized cumulative distribution functions and measures an associated significance level of rejecting the null hypothesis. In Figure 18, we plot the individual differential and cumulative distribution functions for each morphological parameter for the `Full`$_{\rm NUV}$ and `Stellar Mass`$_{\rm NUV}$ green and purple samples. For the KS Statistic, if the probability is below either a 1% or 5% significance level, we can reject the null-hypothesis that the two samples are drawn from a parent distribution at the 2 or 3 sigma levels, respectively.

For the KS tests, we limit the effect of noisy measure-

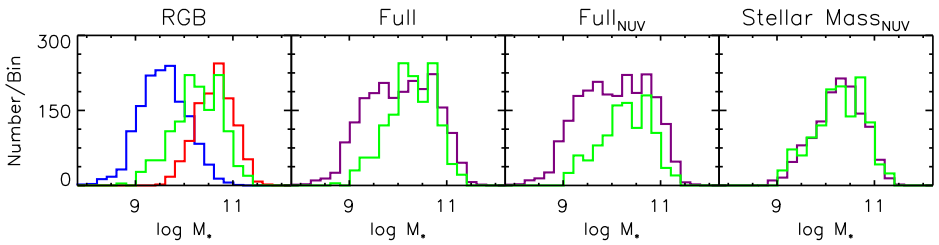

FIG. 14.— Stellar mass distributions for each galaxy sample. The left panel shows the red, green, and blue galaxy samples, while the other panels show various green and purple galaxy samples. For clarity we have weighted the histograms for red and blue galaxies by a factor of half and quarter, respectively.

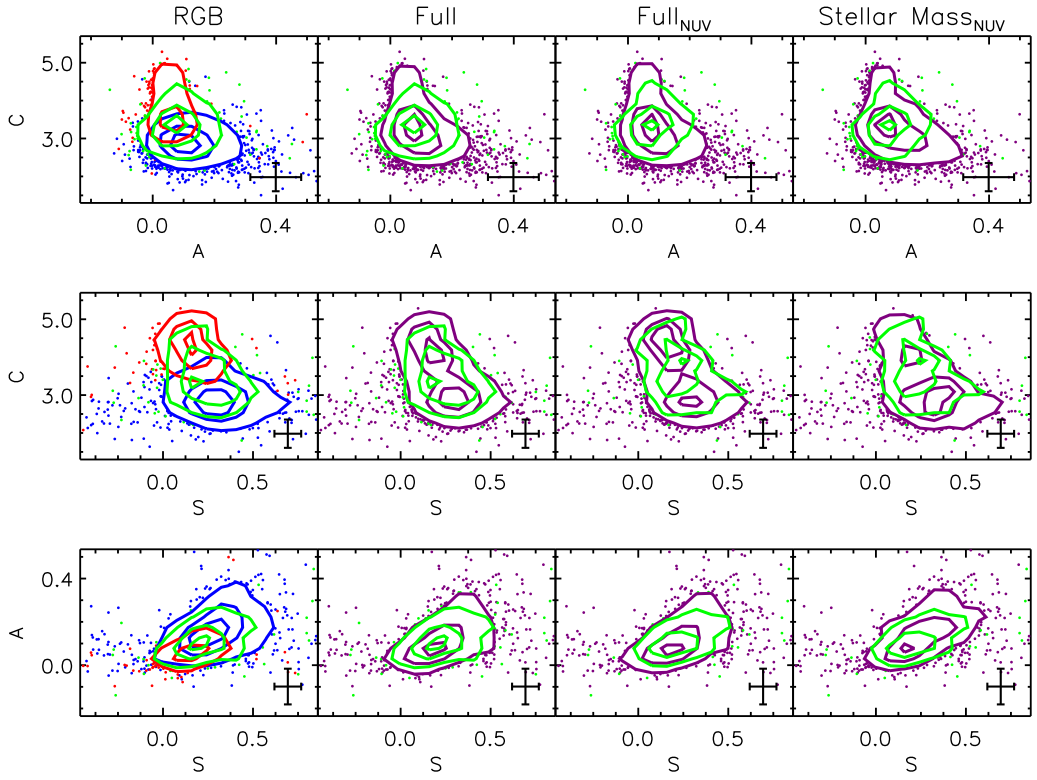

FIG. 15.— *CAS* bivariate distributions shown for `RGB`, `Full`, `Full`$_{NUV}$, and `Stellar Mass`$_{NUV}$ samples. Contours are plotted to contain 30%, 50% and 80% of the galaxies within each sample, with outliers shown as dots outside the 80% contour. Estimates of 1 σ error bars are shown in lower right corner for the median S/N pixel^{-1} of the sample.

ments by applying the test on galaxies only within the parameter ranges shown in Figures 8 and 12 and listed in Table 3. We report the measured significance levels of the KS test results in Table 3. For each morphological parameter (as well as stellar mass and size), we compare the respective green and purple samples and highlight in Table 3 the parameters that we can reject at the 5% significance level in light grey and at the 1% significance level in dark grey. Thus parameters highlighted in dark gray have therefore been rejected at the 3σ level as being drawn from the same parent distribution. These include concentration for all of the `Full`, `Full`$_{NUV}$, and `Stellar Mass`$_{NUV}$ comparison samples, as well as size (r_p) for the `Full` sample and M_{20} and M'_{20} for the `Full`$_{NUV}$ sample. At the 2σ level we can reject B/T for the Full sample and A, B/T, M_{20} and M'_{20} for the `Stellar Mass`$_{NUV}$ sample.

We additionally performed KS tests to compare the morphological distributions of red and green, blue and green, and the union of red and blue to green samples, but we do not include them here as they are all rejected at the 1% level. Smoothness, asymmetry, and the Gini coefficient in the union of red and blue compared with green sample tests were not rejected by the KS test.

6.6. *Morphological Type Comparison using Gini/M_{20}*

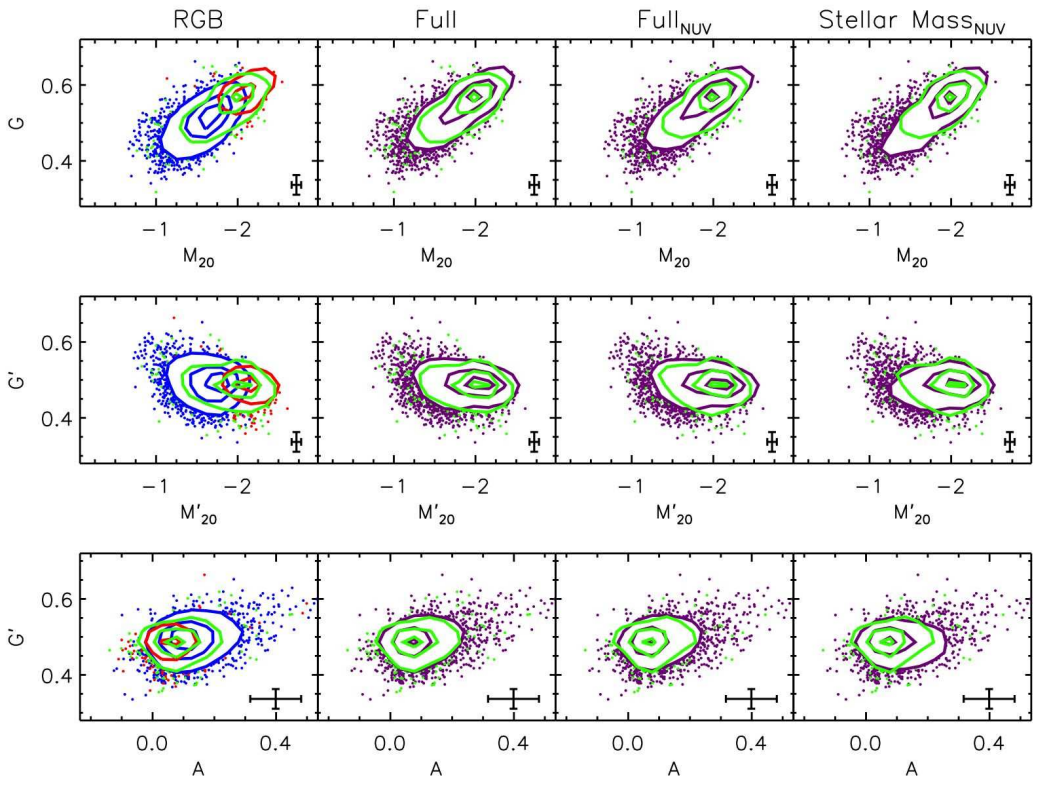

FIG. 16.— G-M_{20}, $G' - M'_{20}$, and G'-A bivariate distributions shown for `RGB`, `Full`, `Full`$_{NUV}$, and `Stellar Mass`$_{NUV}$ samples. Contours and error bars are similar to Figure 15

We repeat the classification of galaxies into rough morphological types (early-type, late-type, or merger) using their location in G/M_{20} space. Table 4 contains the fraction of green and purple galaxies in each sample associated with each morphological type. As before, error bars include both Poisson errors as well as Monte Carlo simulations of the scatter due to measurements errors of G/M_{20}. We do not find that the morphological type fractions are statistically different (at the 2σ level) between any of the green and purple comparison samples.

7. SUMMARY AND DISCUSSION

In this study we find that galaxies in the green valley at $0.4 < z < 1.2$ are an intermediate population between galaxies in the blue cloud and red sequence in terms of morphological type, concentration, asymmetry, smoothness, and merger fraction. Our results do not change if we select green valley galaxies using (NUV-R) color instead of (U-B) color. Using morphological types defined by G/M_{20}, we find that the merger fraction (14%), fraction of late-type galaxies (51%), and early-type galaxies (35%) in the green valley to be intermediate between the red and blue galaxy populations. We show that at a given stellar mass, green galaxies have higher concentration values and lower asymmetry and smoothness values than blue galaxies. They also have lower concentration values and higher asymmetry and smoothness values than red galaxies, at a given stellar mass. Additionally, 12% of our green galaxy sample is bulge-less, with $B/T = 0$. Our results show that green galaxies are generally massive ($M_* \sim 10^{10.5}\ M_\odot$) disk galaxies with high concentrations. Below we discuss the implications of these results.

7.1. *Do green valley galaxies constitute a distinct population?*

The idea that the bulk of the green valley galaxies are a transition population is clearly substantiated by our study of their morphological distribution compared to red sequence and blue cloud galaxies. While our optical color distribution is similarly fit by the two Gaussian distribution of Baldry et al. (2004), we find that galaxies in the green valley have significant morphological differences when compared to red and blue galaxies. This remains true if a UV-optical color selection is used instead.

An important issue when interpreting the observed color bimodality of the CMD is that optical colors reflect not only the star formation history of a galaxy but also its dust content. The degeneracy between star formation history and dust can be partially corrected using the SED modeling (particularly the UV color, e.g. Salim et al. 2007), the Balmer decrement (e.g. Hopkins et al. 2001; Brinchmann et al. 2004), or the IR to UV ratio (e.g. Buat et al. 2005). In contrast to claims that at higher redshifts there may not be a population of transition

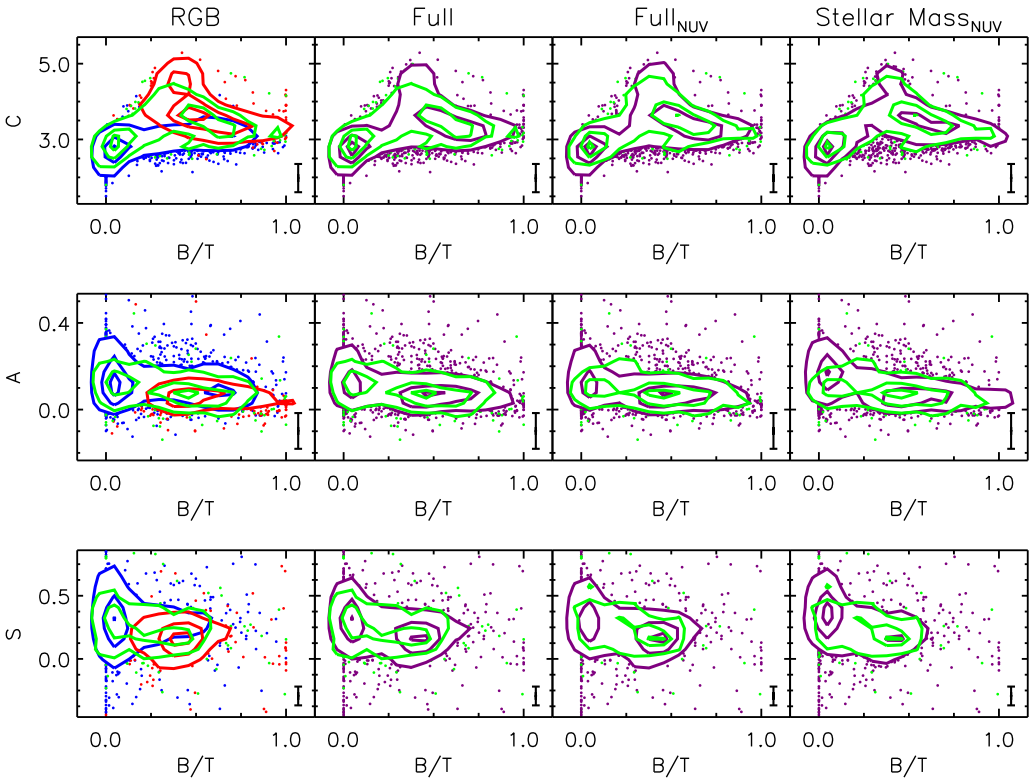

FIG. 17.— *B/T-CAS* bivariate distributions shown for `RGB`, `Full`, `Full`$_{NUV}$, and `Stellar Mass`$_{NUV}$ samples. Contours and error bars are similar to Figure 15

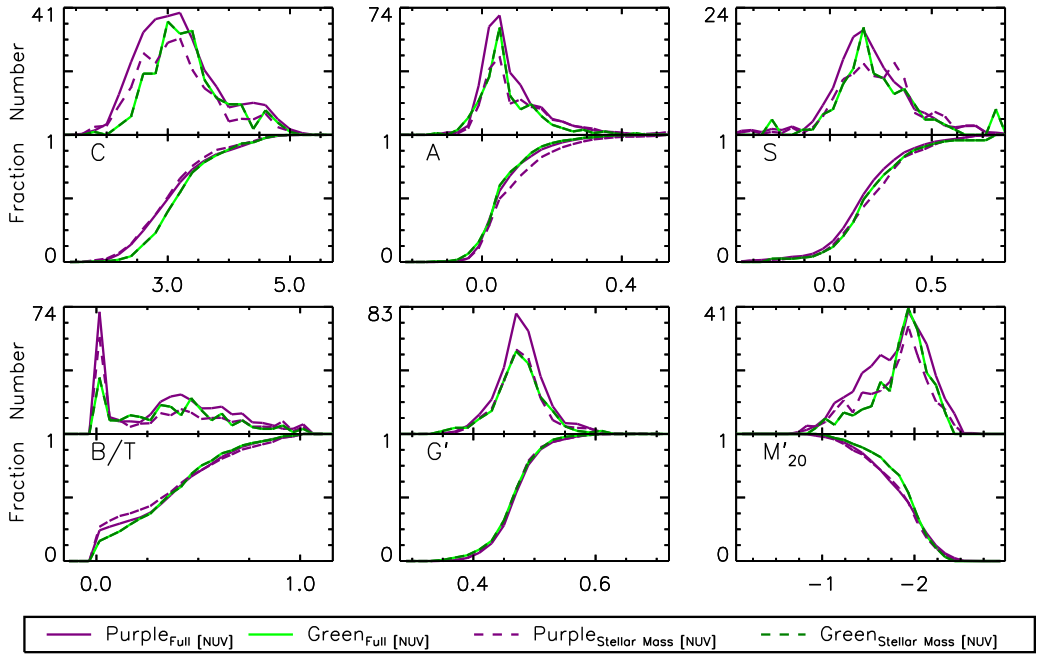

FIG. 18.— One-dimensional differential and cumulative distribution functions for the Full$_{NUV}$ and Stellar Mass$_{NUV}$ green and purple galaxy samples in C, A, S, B/T, G', and M'_{20} space. KS tests are performed for each of these comparison samples; the results are given in Table 3.

galaxies in the green valley (e.g. Brammer et al. 2009), we find that at $0.4 < z < 1.2$ in optically-selected samples there is a distinct population of galaxies that are green not due to dust obscuration but because they have an intermediate age stellar population (see also Salim et al. 2009). As we discuss in Section 6.2, while some galaxies in our green valley sample are green from large SFRs and dust obscuration, our results do not change if they are removed from the sample.

In addition to showing that green galaxies have different morphological distributions than either the red or blue galaxy populations alone, we further compare with control samples of joint red and blue galaxies with the same stellar mass. Our goal is to test whether the green galaxy population has a distinct distribution in any of our quantitative morphological measures than this joint set. This is difficult to test with the green galaxy sample being transition objects by nature and therefore having intermediate properties between the red and blue galaxy samples and is therefore a more stringent test. It is of course subject to errors and noise in the measured morphological parameters, and therefore a null result does not necessarily imply that there is not a difference; rather it may be hard to discern with these kinds of measurements. Additionally, the existence of other non-transition populations within the green galaxy population would only lessen the statistical differences detected between the green galaxy and comparison samples. However, we do find a 3σ difference in terms of the distributions of concentration values and weaker 2σ difference in the B/T, asymmetry, M_{20}, and G' distributions. Therefore it does appear that green galaxies must be a distinct population.

7.2. *What mechanisms are quenching star formation in green valley galaxies?*

Given that the green galaxy population is a transition population between the blue cloud and red sequence in which star formation was recently (within the last $\sim$ Gyr) quenched, it is the ideal population with which to study the quenching mechanism(s) at work. Merger-induced starbursts, which may quickly quench star formation, imprint high asymmetry and G' values on the galaxies. Importantly, we do *not* find that most galaxies in the green valley are experiencing on-going mergers. In fact, the fraction of green galaxies identified as mergers using G/M_{20} (and the fraction with high asymmetry, which is also often used to identify mergers) is *lower* than the fraction within the blue galaxy population. If many of the green valley galaxies have recently undergone merger events, they must be at least $\sim$0.4 Gyr past the merger stage to not be identified using either G/M_{20} or asymmetry (Lotz et al. 2010). Furthermore, 51% of the green galaxies in our sample are identified as late-type and either have not experienced a major merger recently or, if they did, it must have been gas rich (Cox et al. 2008). However, using both quantitative measures to identify mergers, we find that the merger fraction is lower than that of blue galaxies and higher than that of red galaxies. While Kartaltepe et al. (2010) find that most luminous infrared galaxies at $z \sim 1$ are mergers, we do not find that most optically-selected galaxies at these redshifts, even those in the green valley, are identified as mergers.

Additionally, we find that 12% of green galaxies are bulge-less, with $B/T = 0$. As a comparison, 30% of blue galaxies and no red galaxies in our sample have $B/T = 0$. The fact that 12% of the green galaxies are bulge-less raises the question of how these green galaxies were created. Most(64%) of these galaxies are not green due to dust obscuration, as they have low SSFR indicative of intermediate age stellar populations. It is very unlikely that these galaxies have had major mergers in their recent past (which presumably would have built up a bulge component), and we have visually verified that they do not have central point sources indicative of an AGN, which could have biased the measured B/T values. Somehow star formation must have been quenched in these objects without mechanisms that would also lead to the creation of a bulge.

Higher concentration values seen in green galaxies could point to the presence of bars or other internal secular processes that slowly build a central bulge while allowing the disk structure to remain intact. In this scenario a gas-rich galaxy forms a stellar bar that funnels gas to the center of the galaxy, causing enhanced star formation and leading to the development of a bulge. This would increase the concentration measurement of these galaxies, though it does not explain the fraction of bulge-less green valley galaxies discussed above. Sheth et al. (2005) find that there is clear evidence of more centrally-concentrated molecular gas distributions in barred spirals, supporting bar-driven transport of molecular gas to the central kiloparsec of galaxies. Barred spirals of late Hubble-types are less centrally concentrated than early Hubble-types, and there is enhanced star formation activity observed in early Hubble-type bars, indicating higher mass accretion rates (Jogee, Scoville, & Kenney 2005; Kormendy & Kennicutt 2004). Secular processes may also lead to some of the clumpiness that is seen in the profiles of green galaxies.

The stellar disks of green galaxies do not appear to be truncated as they have similar, if not larger, sizes than blue galaxies, as indicated by their large Petrosian radii, which could be due to differences in their stellar mass distribution and the mass-size relationship (e.g. Shen et al. 2003) The tail of green galaxies with particularly large radii could reflect triggered star formation in the outer disks of these galaxies, possibly resulting from galaxy-galaxy interactions for a fraction of the sample. Green valley galaxies do not appear to be fading disks; the higher concentration values point to a different process. Fading disks would also produce higher B/T values, which are not clearly seen here at a given stellar mass (though can not be ruled out by our data). This likely means that simple gas exhaustion is not the dominant mechanism.

There may be a variety of quenching mechanisms responsible for the migration of galaxies from the blue cloud to the red sequence. While major mergers may play a role for some galaxies, we conclude that either a mild external process, such as galaxy harassment or tidal forces, or quite likely an internal process such as the creation of bars, is responsible for the quenching of star formation in many of green valley galaxies at $z \sim 1$.

We thank our anonymous referee for useful comments that have greatly improved this paper. We thank James

TABLE 4
PURPLE G/M_{20} MORPHOLOGICAL TYPES [a]

	Full		Full $_{NUV}$		Stellar Mass$_{NUV}$	
	Green	Purple	Green	Purple	Green	Purple
Mergers	14 ± 2 %	16 ± 2 %	15 ± 3 %	16 ± 2 %	15 ± 3 %	15 ± 3 %
Early Type	35 ± 4 %	34 ± 3 %	39 ± 5 %	36 ± 3 %	39 ± 5 %	34 ± 5 %
Late Type	51 ± 5 %	50 ± 4 %	46 ± 6 %	48 ± 4 %	46 ± 6 %	51 ± 6 %

[a] Percents of each morphological type for each galaxy comparison sample, from G/M_{20} classification for $0.4 < z \leq 1.2$. Uncertainties in each value are from Poisson errors and Monte Carlo Simulated Signal to Noise scatter using Median G/M_{20} errors from Lotz et al. (2006).

Aird, TJ Cox, Aleks Diamond-Stanic, Jacqueline van Gorkom, and Jim Gunn for helpful suggestions and discussions. We use data from the DEEP2 survey, which was supported by NSF AST grants AST00-71048, AST00-71198, AST05-07428, AST05-07483, AST08-07630, AST08-08133. This study makes use of data from AEGIS Sruvey and in particular uses data from *GALEX*, *HST*, Keck, and CFHT. The AEGIS Survey was supported in part by the NSF, NASA, and the STFC. Based on observations obtained with MegaPrime/MegaCam, a joint project of CFHT and CEA/DAPNIA, at the Canada-France-Hawaii Telescope (CFHT) which is operated by the National Research Council (NRC) of Canada, the Institut National des Science de lUniversof the Centre National de la Recherche Scientifique (CNRS) of France, and the University of Hawaii. This work is based in part on data products produced at TERAPIX and the Canadian Astronomy Data Centre as part of the Canada-France-Hawaii Telescope Legacy Survey, a collaborative project of NRC and CNRS.

REFERENCES

Abadi, M. G., Moore, B., & Bower, R. G. 1999, MNRAS, 308, 947
Abraham, R. G., et al. 1994, ApJ, 432, 75
Abraham, R. G., van den Bergh, S., & Nair, P. 2003, ApJ, 588, 218
Baldry, I. K., et al. 2004, ApJ, 600, 681
Ball, N. M., et al. 2006, MNRAS, 373, 845
Balogh, M. L., Navarro, J. F., & Morris, S. L. 2000, ApJ, 540, 113
Barnes, J. E., & Hernquist, L. 1992, ARA&A, 30, 705
Barnes, J. E., & Hernquist, L. 1996, ApJ, 471, 115
Bell, E. F., et al. 2004, ApJ, 608, 752
Bell, E. F., et al. 2006, ApJ, 652, 270
Bell, E. F., & de Jong, R. S. 2001, ApJ, 550, 212
Bell, E. F., McIntosh, D. H., Katz, N., & Weinberg, M. D. 2003, ApJS, 149, 289
Bershady, M. A., Jangren, A., & Conselice, C. J. 2000, AJ, 119, 2645
Bertin, E., & Arnouts, S. 1996, A&AS, 117, 393–404
Birnboim, Y., & Dekel, A. 2003, MNRAS, 345, 349
Birnboim, Y., Dekel, A., & Neistein, E. 2007, MNRAS, 380, 339
Blanton, M. R. 2006, ApJ, 648, 268
Blanton, M. R., et al. 2003, ApJ, 594, 186
Blanton, M. R., & Moustakas, J. 2009, ARA&A, 47, 159
Blanton, M. R., & Roweis, S. 2007, AJ, 133, 734
Bower, R. G., et al. 2006, MNRAS, 370, 645
Brammer, G. B., et al. 2009, ApJ, 706, L173
Brinchmann, J., et al. 2004, MNRAS, 351, 1151
Brooks, A. M., et al. 2009, ApJ, 694, 396
Brown, M. J. I., et al. 2007, ApJ, 654, 858
Bruzual, G., & Charlot, S. 2003, MNRAS, 344, 1000
Buat, V., et al. 2005, ApJ, 619, L51
Bundy, K., et al. 2008, ApJ, 681, 931
Bundy, K., et al. 2010, ApJ, 719, 1969
Cameron, E., et al. 2010, MNRAS, 409, 346
Cardamone, C. N., et al. 2010, ApJ, 721, L38
Coil, A. L., et al. 2008, ApJ, 672, 153
Coil, A. L., et al. 2009, ApJ, 701, 1484
Colless, M., et al. 2001, MNRAS, 328, 1039
Conselice, C. J. 2003, ApJS, 147, 1
Conselice, C. J., Bershady, M. A., & Jangren, A. 2000, ApJ, 529, 886
Cooper, M. C., et al. 2006, MNRAS, 370, 198
Cox, T. J., et al. 2006a, MNRAS, 373, 1013
Cox, T. J., et al. 2006b, ApJ, 650, 791
Cox, T. J., et al. 2008, MNRAS, 384, 386
Croton, D. J., et al. 2006, MNRAS, 365, 11
Davé, R., et al. 2001, ApJ, 552, 473
Davis, M., et al. 2007, ApJ, 660, L1
Dekel, A., & Birnboim, Y. 2006, MNRAS, 368, 2
Downes, D., et al. 1996, ApJ, 461, 186
Driver, S. P., et al. 2006, MNRAS, 368, 414
Elmegreen, B. G., Elmegreen, D. M., & Hirst, A. C. 2004, ApJ, 612, 191
Eskridge, P. B., et al. 2000, AJ, 119, 536
Faber, S. M., et al. 2007, ApJ, 665, 265
Farouki, R., & Shapiro, S. L. 1980, ApJ, 241, 928
Farouki, R., & Shapiro, S. L. 1981, ApJ, 243, 32
Gerke, B. F., et al. 2007, MNRAS, 376, 1425
Guillaume, M., et al. 2006, Proc. SPIE, 6064, 332
Gunn, J. E., & Gott, III, J. R. 1972, ApJ, 176, 1
Hernquist, L. 1992, ApJ, 400, 460
Hernquist, L. 1993, ApJ, 409, 548
Hester, J. A. 2006, ApJ, 647, 910–921
Hickox, R. C., et al. 2008, PSAP, 381, 417
Hopkins, A. M., et al. 2001, AJ, 122, 288
Hopkins, P. F., et al. 2006, ApJS, 163, 1
Ilbert, O., et al. 2006, A&A, 457, 841
Jogee, S., et al. 2004, ApJ, 615, L105
Jogee, S., Scoville, N., & Kenney, J. D. P. 2005, ApJ, 630, 837
Johansson, P. H., Naab, T., & Ostriker, J. P. 2009, ApJ, 697, L38
Kang, X., Jing, Y. P., & Silk, J. 2006, ApJ, 648, 820
Kartaltepe, J. S., et al. 2010, ApJ, 721, 98
Kauffmann, G., et al. 2003, MNRAS, 341, 33
Kereš, D., et al. 2005, MNRAS, 363, 2
Kereš, D., et al. 2009, MNRAS, 396, 2332
Kimm, T., et al. 2009, MNRAS, 394, 1131
Kormendy, J., & Kennicutt, Jr., R. C. 2004, ARA&A, 42, 603
Kriek, M., et al. 2008, ApJ, 682, 896
Larson, R. B., Tinsley, B. M., & Caldwell, C. N. 1980, ApJ, 237, 692
López-Sanjuan, C., et al. 2010a, ApJ, 710, 1170
López-Sanjuan, C., et al. 2010b, ArXiv e-prints
Lotz, J. M., et al. 2006, ApJ, 636, 592
Lotz, J. M., et al. 2008a, MNRAS, 391, 1137
Lotz, J. M., et al. 2008b, ApJ, 672, 177
Lotz, J. M., et al. 2010, MNRAS, 404, 575
Lotz, J. M., Primack, J., & Madau, P. 2004, AJ, 128, 163
Madgwick, D. S., et al. 2002, MNRAS, 333, 133
Martin, D. C., et al. 2005, ApJ, 619, L1
Martin, D. C., et al. 2007, ApJS, 173, 342
Masters, K. L., et al. 2010, MNRAS, 405, 783
McNamara, B. R., et al. 2000, ApJ, 534, L135
McNamara, B. R., et al. 2001, ApJ, 562, L149
McNamara, B. R., & Nulsen, P. E. J. 2007, ARA&A, 45, 117
Menéndez-Delmestre, K., et al. 2007, ApJ, 657, 790
Mihos, J. C., & Hernquist, L. 1994, ApJ, 425, L13
Moore, B., et al. 1996, Nature, 379, 613
Moore, B., Lake, G., & Katz, N. 1998, ApJ, 495, 139
Morrissey, P., et al. 2007, ApJS, 173, 682
Naab, T., & Burkert, A. 2003, ApJ, 597, 893
Nandra, K., et al. 2007, ApJ, 660, L11
Oesch, P. A., et al. 2010, ApJ, 714, L47
Pannella, M., et al. 2009, ApJ, 701, 787
Pierce, C. M., et al. 2010, MNRAS, 408, 139
Quilis, V., Moore, B., & Bower, R. 2000, Science, 288, 1617

Regan, M. W., Sheth, K., & Vogel, S. N. 1999, ApJ, 526, 97
Robertson, B., et al. 2006, ApJ, 645, 986
Salim, S., et al. 2007, ApJS, 173, 267
Salim, S., et al. 2009, ApJ, 700, 161
Salim, S., & Rich, R. M. 2010, ApJ, 714, L290
Scarlata, C., et al. 2007, ApJS, 172, 406
Schawinski, K., et al. 2009, ApJ, 690, 1672
Sellwood, J. A., & Wilkinson, A. 1993, Reports on Progress in Physics, 56, 173
Sersic, J. L. 1968. Atlas de galaxias australes
Shen, S., et al. 2003, MNRAS, 343, 978
Sheth, K., et al. 2000, ApJ, 532, 221
Sheth, K., et al. 2005, ApJ, 632, 217
Sheth, R. K., et al. 2003, ApJ, 594, 225
Sheth, R. K., & Tormen, G. 2002, MNRAS, 329, 61
Simard, L., et al. 2002, ApJS, 142, 1
Springel, V., Di Matteo, T., & Hernquist, L. 2005a, ApJ, 620, L79
Springel, V., Di Matteo, T., & Hernquist, L. 2005b, MNRAS, 361, 776
Steinmetz, M., & Navarro, J. F. 2002, New Astronomy, 7, 155
Strateva, I., et al. 2001, AJ, 122, 1861
Takamiya, M. 1999, ApJS, 122, 109
Tinker, J. L., Wechsler, R. H., & Zheng, Z. 2010, ApJ, 709, 67
Toomre, A. 1977, ARA&A, 15, 437
Toomre, A., & Toomre, J. 1972, ApJ, 178, 623
van den Bosch, F. C., et al. 2008, MNRAS, 387, 79
Weiner, B. J., et al. 2005, ApJ, 620, 595
Weiner, B. J., et al. 2009, ApJ, 692, 187
Williams, R. J., et al. 2009, ApJ, 691, 1879
Willmer, C. N. A., et al. 2006, ApJ, 647, 853
Wyder, T. K., et al. 2007, ApJS, 173, 293
York, D. G., et al. 2000, AJ, 120, 1579
Zamojski, M. A., et al. 2007, ApJS, 172, 468
Zhu, G., Blanton, M. R., & Moustakas, J. 2010, ApJ, 722, 491